Since January 2020 Elsevier has created a COVID-19 resource centre with free information in English and Mandarin on the novel coronavirus COVID-19. The COVID-19 resource centre is hosted on Elsevier Connect, the company's public news and information website.

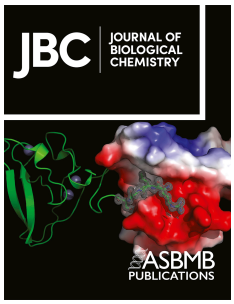

Transmembrane serine protease TMPRSS2 implicated in SARS-CoV-2 infection is autoactivated intracellularly and requires N-glycosylation for regulation

Yikai Zhang, Shijin Sun, Chunyu Du, Kaixuan Hu, Ce Zhang, Meng Liu, Qingyu Wu, Ningzheng Dong

PII: S0021-9258(22)01086-9

DOI: https://doi.org/10.1016/j.jbc.2022.102643

Reference: JBC 102643

To appear in: *Journal of Biological Chemistry*

Received Date: 1 July 2022

Revised Date: 19 October 2022

Accepted Date: 20 October 2022

Please cite this article as: Zhang Y, Sun S, Du C, Hu K, Zhang C, Liu M, Wu Q, Dong N, Transmembrane serine protease TMPRSS2 implicated in SARS-CoV-2 infection is autoactivated intracellularly and requires N-glycosylation for regulation, *Journal of Biological Chemistry* (2022), doi: https://doi.org/10.1016/j.jbc.2022.102643.

Research Article

Transmembrane serine protease TMPRSS2 implicated in SARS-CoV-2 infection is autoactivated intracellularly and requires N-glycosylation for regulation

Yikai Zhang[1], Shijin Sun[1], Chunyu Du[1,2], Kaixuan Hu[1,2], Ce Zhang[1], Meng Liu[1], Qingyu Wu[1,*], and Ningzheng Dong[1,2,*]

From the [1]Cyrus Tang Hematology Center, Collaborative Innovation Center of Hematology, State Key Laboratory of Radiation Medicine and Prevention, Suzhou Medical College, Soochow University, Suzhou, China; the [2]MOH Key Laboratory of Thrombosis and Hemostasis, Jiangsu Institute of Hematology, the First Affiliated Hospital of Soochow University, Suzhou, China.

Running title: TMPRSS2 activation and N-glycosylation

*For correspondence: Qingyu Wu, wuqy@suda.edu.cn; Ningzheng Dong, ningzhengdong@suda.edu.cn

Abstract

Transmembrane protease serine 2 (TMPRSS2) is a membrane-bound protease expressed in many human epithelial tissues, including the airway and lung. TMPRSS2-mediated cleavage of viral spike (S) protein is a key mechanism in severe acute respiratory syndrome (SARS) coronavirus (CoV)-2 activation and host cell entry. To date, the cellular mechanisms that regulate TMPRSS2 activity and cell surface expression are not fully characterized. In this study, we examined two major posttranslational events, zymogen activation and N-glycosylation, in human TMPRSS2. In experiments with human embryonic kidney 293 (HEK293), bronchial epithelial 16HBE, and lung alveolar epithelial A549 cells, we found that TMPRSS2 was activated via intracellular autocatalysis and that this process was blocked in the presence of hepatocyte growth factor activator inhibitors 1 and 2. By glycosidase digestion and site-directed mutagenesis, we showed that human TMPRSS2 was N-glycosylated. N-glycosylation at an evolutionarily conserved site in the scavenger receptor cysteine-rich domain was required for calnexin-assisted protein folding in the ER and subsequent intracellular trafficking, zymogen activation, and cell surface expression. Moreover, we showed that TMPRSS2 cleaved SARS-CoV-2 S protein intracellularly in HEK293 cells. These results provide new insights into the cellular mechanism in regulating TMPRSS2 biosynthesis and function. Our findings should help to understand the role of TMPRSS2 in major respiratory viral diseases.

Keywords: HAI-1; HAI-2; N-glycosylation; SARS-CoV-2; spike protein; TMPRSS2; TTSP; zymogen activation

Introduction

Transmembrane protease serine 2 (TMPRSS2) is a member of the type II transmembrane serine protease (TTSP) family (1-3), which includes hepsin, matriptase, human airway trypsin-like protease (HAT), and corin that are of physiological importance (4-11). TMPRSS2 is expressed in many epithelial tissues, including the prostate, trachea, bronchus, lung, kidney, small intestine, colon, pancreas, thymus, and salivary glands (12-14). To date, the physiological function of TMPRSS2 remains elusive. In mice, disruption of the *Tmprss2* gene does not cause noticeable changes in embryonic development, postnatal survival, fertility, prostate morphology, and kidney function (15). In humans, *TMPRSS2* overexpression and gene rearrangements have been identified as an underlying mechanism in prostate cancer development and progression (16-18).

TTSPs are anchored on the cell surface via an N-terminal transmembrane domain (2,3). In human airways, TTSPs are exploited by coronaviruses (CoVs), including the severe acute respiratory syndrome (SARS) CoV, the Middle East respiratory syndrome (MERS) CoV, and SARS-CoV-2, for their infectivity. In these CoVs, spike (S) proteins on the viral envelop are responsible for cellular receptor binding, membrane fusion, and cell entry (19-21). Proteolytic cleavage of S proteins by host TTSPs, including HAT, TMPRSS2, TMPRSS4, TMPRSS11A, and TMPRSS11E, enhances S protein activity and CoV infection (22-27).

To date, ample evidence indicates that TMPRSS2-mediated S protein cleavage is a critical mechanism in SARS-CoV-2 activation and cell entry. In cultured human lung epithelial cells, TMPRSS2 expression enhances SARS-CoV-2 infection, whereas inhibition of TMPRSS2 expression or activity blocks the viral entry (28-31). In a mouse *Tmprss2* knockout model, SARS-CoV-2 infection in the lung is markedly reduced compared to that in wild-type (WT) mice (32). Similarly, a small-molecule TMPRSS2 inhibitor is shown to provide prophylactic and therapeutic benefit in a mouse model of severe COVID-19 (33). In addition to SARS-CoV-2, TMPRSS2 also enhances the activity of SARS and MERS CoVs and influenza A viruses by

cleaving S proteins and hemagglutinins, respectively (13,22,34-36). These data underscore a key role of TMPRSS2 in major viral respiratory diseases.

Most TTSPs are synthesized in a single-chain zymogen form. Posttranslational modifications, including N- or O-glycosylation, zymogen activation, phosphorylation, and ectodomain cleavage, are important mechanisms in regulating TTSP activities (37-45). Previous studies indicate that TMPRSS2 is synthesized as a single-chain zymogen and activated by autocatalysis (46). To date, the cellular mechanism that regulates TMPRSS2 activation and cell surface expression is not fully understood. In this study, we examined TMPRSS2 zymogen activation and N-glycosylation in biochemical and cellular experiments. Our results show that TMPRSS2 is activated intracellularly by autocatalysis in human kidney, airway, and lung-derived cells and that N-glycosylation in the scavenger receptor cysteine-rich (SRCR) domain is critical for TMPRSS2 activation and cell surface expression. We also show that TMPRSS2 cleaves SARS-CoV-2 S protein intracellularly. These findings help to understand the cellular mechanism underlying TMPRSS2 activation and function.

Results

TMPRSS2 autoactivation in human cells

Figure 1A is an illustration of human TMPRSS2 protein domains, including an N-terminal cytoplasmic tail, a transmembrane domain (TM), a low-density lipoprotein receptor (LDLR)-like domain, an SRCR domain, and a C-terminal trypsin-like protease domain with three canonical active sites, His333 (H333), Asp382 (D382), and Ser478 (S478). The conserved zymogen activation site is at R292-I293. There is a disulfide bond between the propeptide and the protease domain (Fig. 1*A*). To study TMPRSS2, we transfected human embryonic kidney 293 (HEK293) cells with a plasmid expressing human TMPRSS2 with a C-terminal V5 tag (Fig. 1*A*). In western blotting of lysates from the transfected cells, we detected a single band of ~65 kDa under non-reducing conditions (Fig. 1*B*, *left panel* and Fig. S1*A*). Under reducing conditions, we detected an ~65-kDa band and an ~31-kDa band (Fig. 1*B*, *right panel* and Fig.

S1*A*), representing the zymogen and the cleaved protease domain fragment, respectively (Fig. 1*A*). Because the V5 tag was at the C-terminus, the cleaved N-terminal fragment was not detected. There were two additional lighter bands of ~45-48 kDa, probably generated by cleavages between the LDLR and the SRCR domains.

To understand how the TMPRSS2 fragments were generated, we made TMPRSS2 R292A and S478A mutants, in which the canonical activation site (Fig. 1*C*) and the catalytic serine (Fig. 1*D*) were mutated, respectively. Both the mutants are expected to be catalytically inactive. We expressed TMPRSS2 WT and the mutants R292A and S478A in HEK293 cells. In western blotting under reducing conditions, we detected the ~65-kDa, but not the ~31-kDa, band in the mutants R292A and S478A (Fig. 1*E*, *left panel* and Fig. S1*B*). Similar results were found when the WT and the mutants were expressed in human bronchial epithelial 16HBE cells (Fig. 1*E*, *middle panel* and Fig. S1*B*) and human alveolar basal epithelial A549 cells (Fig. 1*E*, *right panel* and Fig. S1*B*). These results indicated that the ~31-kDa band is the protease domain cleaved at R292 and that the cleavage depends on the catalytic activity of TMPRSS2.

To verify these results, we examined the catalytic activity of TMPRSS2 expressed in HEK293 cells. In a fluorogenic substrate assay, significant catalytic activity was detected in the cells expressing the TMPRSS2 WT, whereas little activity was found in the vector-transfected cells or the cells expressing the mutants R292A and S478A (Fig. 1*F*). These results are consistent, indicating that the TMPRSS2 WT is activated in HEK293 cells.

TMPRSS2 expression on the cell surface

A type II transmembrane protein, TMPRSS2 is expected to be on the cell surface. To verify its cell surface location, we biotin-labeled membrane proteins in HEK293 cells and analyzed TMPRSS2 proteins by western blotting. Surprisingly, we detected the mutants R292A and S478A, but not the WT, in biotin-labeled protein fractions (Fig. S2*A*, *left panel*). In cell lysates, levels of the WT and the mutants were comparable (Fig. S2*A*, *right panel*). We confirmed

these results by flow cytometry, which showed the mutants, but not the WT, on the HEK293 cell surface (Fig. S2*B*). Moreover, we observed immunostaining of the mutants, but not the WT, in non-permeabilized HEK293 cells, whereas immunostaining of the WT and the mutants was observed in permeabilized HEK293 cells (Fig. S2*C*). Considering the above experiments were done using an anti-C-terminal V5 tag antibody, it is possible that the activated TMPRSS2 WT cleaved the V5 tag, preventing the antibody detection, whereas in the inactive mutants R292A and S478A, the V5 tag was not cleaved and thus detectable.

To verify this hypothesis, we tested another antibody against an extracellular stem region of human TMPRSS2. (The specific epitope was undisclosed by the commercial maker.) In flow cytometry, the antibody detected the TMPRSS2 WT and the mutants R292A and S478A on the HEK293 cell surface (Fig. 2*A*). Levels of the cell surface WT were lower than those of the mutants (Fig. 2*B*), probably due to ectodomain shedding of the WT. In immunostaining, the WT and the mutants were detected on the surface of non-permeabilized and within permeabilized HEK293 cells (Fig. 2*C*). Similarly, the cell surface expression of the WT and the mutants was detected in human airway 16HBE and lung A549 cells by immunostaining (Fig. 2*D*) and flow cytometry (Fig. S3, *A* and *B*).

Intracellular activation of TMPRSS2

To understand the subcellular location of TMPRSS2 activation, we treated HEK293 cells expressing the TMPRSS2 WT with trypsin to remove surface proteins and lysed the cells for western blotting under reducing conditions. We detected the ~65-kDa zymogen band and the ~31-kDa protease domain band in the cells with or without trypsin digestion (Fig. 3*A*). In control experiments with corin, a cardiac TTSP that is activated on the cell surface but not intracellularly (39,47), the ~40-kDa cleaved protease domain band disappeared after the cells were treated with trypsin (Fig. 3*B*). These results showed that, unlike corin, TMPRSS2 is activated inside the cell.

We then treated the TMPRSS2-expressing HEK293 cells with monensin and brefeldin A (BFA), which inhibit protein trafficking in the Golgi and the endoplasmic reticulum (ER), respectively (48). In western blotting, we observed similar levels of the ~65- and ~31-kDa bands in the TMPRSS2-expressing cells without or with monensin treatment (up to 0.9 μM) (Fig. 3*C*). In contrast, BFA treatment reduced the level of the ~31-kDa protease domain band dose-dependently (Fig. 3*D*). In control experiments with corin, the 40-kDa protease domain band was undetectable in the monensin- (Fig. 3*E*) or BFA- (Fig. 3*F*) treated cells, consistent with the extracellular activation of corin (39,47). These results indicated that TMPRSS2 is activated after exiting the ER, most likely in the Golgi, before reaching the cell surface.

Inhibition of TMPRSS2 activation cleavage by HAI-1 and HAI-2

Hepatocyte growth factor activator inhibitors 1 and 2 (HAI-1 and HAI-2) are Kunitz-type inhibitors that inhibit many TTSPs, including TMPRSS2 (49-51). To verify TMPRSS2 intracellular autoactivation, we co-expressed TMPRSS2 and HAI-1 or HAI-2 in HEK293 cells and analyzed TMPRSS2 activation by western blotting. We found that the TMPRSS2 activation cleavage was abolished in the HEK293 cells co-expressing HAI-1 or HAI-2, as indicated by the absence of the ~31-kDa protease domain band (Fig. 4). These results indicated that inhibition of TMPRSS2 activity by HAI-1 or HAI-2 prevents TMPRSS2 intracellular autoactivation in HEK293 cells.

Effects of N-glycosylation on TMPRSS2 activation

N-glycosylation is an important mechanism in the regulation of TTSP folding, intracellular trafficking, and zymogen activation (41,52,53). However, the functionality of individual N-glycans in a particular protein is hard to predict. There are two predicted N-glycosylation sites in human TMPRSS2, one at N250 in the SRCR domain and other at N286 before the protease domain (Fig. 5*A*). To test if TMPRSS2 is N-glycosylated, we treated lysates from the TMPRSS2-expressing cells with peptide-N-glycosidase F (PNGase F) to remove N-glycans from glycoproteins. In western blotting, the ~65-kDa TMPRSS2 zymogen band migrated faster

at ~59 kDa after the PNGase F treatment, whereas the position of the ~31-kDa protease domain band remained unchanged (Fig. 5*B*). Similarly, western blotting of human lung A549 cell lysates showed that endogenous TMPRSS2 migrated faster when the samples were treated with PNGase F (Fig. S4). These results indicated that TMPRSS2 is N-glycosylated in the propeptide region.

To verify these results and understand the effect of N-glycosylation on TMPRSS2 activation, we made mutants N250Q, N286Q, and N250Q/N286Q, in which the N-glycosylation consensus sequences were mutated, individually or together (Fig. 5*A*). We expressed the mutants in HEK293 cells and analyzed them in western blotting. The zymogen bands from the WT, the mutants N250Q and N286Q, and the mutant N250Q/N286Q migrated at ~65 kDa, ~62 kDa, and ~59 kDa, respectively (Fig. 5*C*). When the lysates containing the WT and the mutants were treated with PNGase F, the zymogen bands all migrated at ~59 kDa (Fig. S5). These results indicated that both N250 and N286 were N-glycosylated. Intriguingly, the ~31-kDa protease domain band was barely detectable in the mutants N250Q and N250Q/N286Q, but stronger in the mutant N286Q compared to that in the WT (Fig. 5, *C* and *D*). These results indicated that N-glycosylation at N250, but not at N286, is necessary for TMPRSS2 activation in HEK293 cells.

Effects of N-glycosylation on TMPRSS2 intracellular trafficking

We next examined the TMPRSS2 WT and the mutants N250Q, N286Q, and N250Q/N286Q on the surface of HEK293 cells. In flow cytometry, levels of the mutants N250Q and N250Q/N286Q were lower than those of the WT and the mutant N286Q (Fig. 5, *E* and *F*), suggesting that abolishing N-glycosylation at N250, but not N286, inhibited TMPRSS2 trafficking to the cell surface. Consistently, the mutant N250Q had a longer intracellular half-life than those of the WT and the mutant N286Q in cycloheximide (CHX)-based protein chase and western blotting experiments (11.7 ± 2.1 *vs.* 4.8 ± 0.8 h in the WT and 6.1 ± 1.6 h in the mutant N286Q, *P* values = 0.004 and 0.011, respectively) (Fig. 6, *A*-*C*). In immunostaining,

strong overlapping staining of the mutant N250Q and the ER marker KDEL was observed in HEK293 cells, whereas such overlapping staining was not observed in WT or the mutant N286Q (Fig. 6*D*, *left column*). In contrast, there was no apparent overlapping staining of the Golgi marker GM130 with the WT or the mutants N250Q and N286Q (Fig. 6*D, right column*). Similar overlapping staining with KDEL, but not GM130, was observed in HEK293 cells expressing the mutant N250Q/N286Q (Fig. S6). These results indicated that abolishing N-glycosylation at N250, but not N286, prevents TMPRSS2 from exiting the ER.

TMPRSS2 N-glycosylation sites in three-dimensional (3-D) models

Using the artificial intelligence-based RoseTTAFold program for protein structure prediction (54), we built 3-D models of the TMPRSS2 extracellular region. The LDLR, the SRCR, and the protease domains were folded as independent modules (Fig. 7*A*). N250 was in an SRCR domain loop away from the protease domain, whereas N286 was in a linker region near the protease domain. Both N250 and N286 were surface exposed (Fig. 7*B*). Substitution of N250 or N286 with Gln residues did not alter the overall 3-D model of the TMPRSS2 extracellular region (Fig. 7, *A* and *B*).

Interaction of TMPRSS2 with ER chaperones

Calnexin binding to N-glycans is an important mechanism in glycoprotein folding (55). N-glycan elimination prevents client protein folding, causing ER retention of poorly folded proteins via direct protein-protein interactions with calnexin and binding immunoglobulin protein (BiP) (52,56). We immunoprecipitated the WT and the mutants N250Q and N286Q in the lysates from HEK293 cells and examined co-precipitated ER chaperones by western blotting (Fig. 8, *A* and *B*). Levels of calnexin and BiP co-precipitated with the mutant N250Q were higher than those with the WT and the mutant N286Q, whereas levels of co-precipitated calreticulin and heat shock protein 70 (two other ER chaperones) were comparable among the WT and the mutants. In controls, similar levels of the WT and the mutants were found in the co-precipitated samples (Fig. 8A, row 5) and in the starting cell lysates (Fig. 8*A*, row 6).

These results are consistent with the observed ER retention of the mutant N250Q, indicating that N-glycosylation at N250, but not N286, in TMPRSS2 is critical for calnexin-mediated folding in the ER.

Effects of glucosidase inhibition on TMPRSS2 activation and interaction with calnexin

In calnexin-mediated folding, triglucosylated oligosaccharides on glycoproteins must be trimmed by α-glucosidases I and II, consecutively, to monoglucosylated oligosaccharides before the calnexin-N-glycan interaction occurs (55). To verify the role of the N-glycans on TMPRSS2 in regulating TMPRSS2 activation and binding to ER chaperones, we incubated the HEK293 cells expressing the WT and the mutants N250Q and N286Q with 1-deoxynojirimycin (DNJ), an inhibitor of α-glucosidases I and II (57,58). In western blotting, we found that the DNJ treatment inhibited TMPRSS2 activation, as indicated by the absence or reduced levels of the ~31-kDa protease domain band in the WT and the mutant N286Q, respectively (Fig. 9*A*). In the co-immunoprecipitation experiment, levels of calnexin and BiP co-precipitated with the WT and the mutant N286Q were increased in the DNJ treated samples, compared with those without the DNJ treatment (Fig. 9, *B* and *C*). In contrast, levels of calnexin and BiP co-precipitated with the mutant N250Q remained high with or without the DNJ treatment (Fig. 9, *B* and *C*). In controls, levels of HSP70 co-precipitated with the WT and the mutants N250Q and N286Q were similar with or without the DNJ treatment. Similar levels of the TMPRSS2 WT and the mutants were verified in the co-precipitated samples (Fig. 9*B*, row 4) and the starting lysates (Fig. 9*B*, row 5). These results indicated that the inhibition of α-glucosidase activities by DNJ prevented the calnexin binding to the N-glycan on the WT and the mutant N286Q, which impaired the calnexin-assisted TMPRSS2 folding in the ER, leading to increased direct protein-protein interactions with calnexin and BiP.

Intracellular cleavage of SARS-CoV-2 S protein by TMPRSS2

Many studies have shown that furin and TMPRSS2 cleave SARS-CoV-2 S protein at the

S1/S2 and S2' sites, respectively (Fig. 10*A*), although alternative furin and TMPRSS2 cleavages have been reported (20,21,59,60). Given the finding of intracellular TMPRSS2 activation, we tested if TMPRSS2 could cleave SARS-CoV-2 S protein intracellularly. We expressed the full-length SARS-CoV-2 S protein in HEK293 cells and prepared cell lysates before and after trypsin treatment. In western blotting, the S and S2 fragments of SARS-CoV-2 S protein were detected (Fig. 10*B*, *lanes 2 and 3*), consistent with the notion that furin, which is abundant in HEK293 cells (61), is primarily responsible for cleaving the S1/S2 site. In HEK293 cells co-transfected with the S protein and TMPRSS2, two additional bands appeared at ~70 and ~66 kDa, respectively (Fig. 10*B*, *lane 4*). These two bands were also observed in the trypsin-treated cells (Fig. 10*B*, *lane 5*), indicating that they were cleaved by TMPRSS2 inside the cells, consistent with the intracellular TMPRSS2 activation observed in our experiments.

To verify the TMPRSS2 cleavage at the S2' site, we made S1/S2 and S2' mutants, in which the furin and TMPRSS2 cleavage sites in the S protein were mutated, respectively (Fig. 10*C*). In western blotting of lysates from transfected HEK293 cells, the S2 fragment in the S1/S2 mutant was barely detectable without or with TMPRSS2 co-transfection (Fig. 10*D*). In contrast, the S2' fragment was detected in the cells co-expressing TMPRSS2 and S protein WT and the S1/S2 mutant, but not the S2' mutant (Fig. 10*D*). In controls, similar levels of TMPRSS2 protein were confirmed in the co-transfected cells (Fig. 10*D*). These results indicated that the observed S2' fragment was derived from TMPRSS2-mediated cleavage at the S2' site.

Discussion

TMPRSS2-mediated S protein cleavage is critical in SARS-CoV-2 infection (20,21). In this study, we examined cellular mechanisms in regulating TMPRSS2 activation and cell surface expression. We expressed the full-length human TMPRSS2, *i.e*., isoform 1, with 529 amino acids, which differs from the originally published human TMPRSS2 isoform 2 with 492 amino

acids (1,62). Compared to TMPRSS2 isoform 2, TMPRSS2 isoform 1 has extra 37 amino acids at the N-terminus, probably due to alternative mRNA splicing. To date, there is no evidence indicating that the cytoplasmic extension may alter TMPRSS2 expression or function.

Zymogen activation is a key step in regulating protease activity. In TTSPs, mechanisms underlying zymogen activation vary considerably. For example, corin (39,47), enteropeptidase (63), matriptase (40,64) are activated extracellularly by proprotein convertase subtilisin/kexin 6, trypsin, and prostasin, respectively. Matriptase-2 and hepsin are self-activated on the cell surface (43,65,66), whereas TMPRSS11A is self-activated in the ER (67). TMPRSS2 autoactivation has been reported (46); however, the specific subcellular location remains unknown. In this study, we confirmed TMPRSS2 autoactivation in HEK293 cells and human airway 16HBE and lung A549 epithelial cells. Moreover, our data indicated that TMPRSS2 is likely activated in the Golgi, *i.e.*, after exiting the ER and before reaching the cell membrane. These results highlight the diversity in zymogen activation mechanisms among TTSPs.

HAI-1 and HAI-2 are inhibitors of many epithelial TTSPs (21,49). In mice, HAI-1 or HAI-2 deficiency causes embryonic lethality due to dysregulated protease activities (68-70). Recently, HAI-1 and HAI-2 have been identified as endogenous TMPRSS2 inhibitors in prostate cancer cells (50). In cell-based experiments, HAI-2 inhibits TMPRSS2-mediated influenza A virus and SARS-CoV-2 infection (51,71). Consistently, co-transfection of HAI-1 or HAI-2 in HEK293 cells blocked TMPRSS2 activation in our study. HAI-1 and HAI-2 are known to act both intracellularly and on the cell surface (44,72,73). If HAI-1 and HAI-2 inhibited TMPRSS2 on the cell surface in our experiments, we should still expect to detect the ~31-kDa protease domain band in cell lysates. In western blotting, however, we did not observe the ~31-kDa band, indicating that TMPRSS2 inhibition by HAI-1 and HAI-2 occurred inside the cells. These data are consistent with intracellular TMPRSS2 activation.

N-glycosylation is a key posttranslational modification in proteins (74). The consensus N-glycosylation sequence is Asn-X-Ser or Asn-X-Thr, where X can be any amino acid but Pro (75). In human TMPRSS2, there are three Asn-X-Ser sequences at 165-167, 250-252, and 286-288 positions, respectively. However, the sequence at 165-167 is Asn-Pro-Ser, which is not an N-glycosylation site. By analyzing the mutants N250Q, N286Q, and N250Q/N286Q, we showed that TMPRSS2 indeed was N-glycosylated at the predicted sites. In TTSPs, the functional importance of the predicted N-glycosylation sites varies extensively. TMPRSS13, for example, has two N-glycosylation sites in its SRCR domain, but those sites are unnecessary for cell surface expression and zymogen activation (41). In contrast, hepsin has one N-glycosylation site in the SRCR domain, which is critical for calnexin-assisted protein folding, ER exiting, cell surface expression, and zymogen activation (53). In this study, we found that the N-glycan at N250 in the SRCR domain of TMPRSS2 appears to have a similar role in calnexin-mediated folding and ER exiting. Elimination of the N-glycan at this site resulted in increased direct protein-protein interactions with calnexin and BiP, ER retention, and impaired intracellular trafficking, zymogen activation, and cell surface expression. As discussed above, TMPRSS2 is likely activated in the Golgi. The observed ER retention could explain impaired zymogen activation of the mutant N250Q. Consistently, treatment of DNJ, which inhibits α-glucosidase activities and hence the calnexin-N-glycan interaction, also blocked the activation of the TMPRSS2 WT and the mutant N286Q in transfected cells.

The phenotypic difference between the mutants N250Q and N286Q is intriguing. Unlike the mutant N250Q, abolishing N-glycosylation at N286 did not impair TMPRSS2 intracellular trafficking, zymogen activation, and cell surface expression. The underlying mechanism is unclear. In our 3-D protein modeling, modules in the TMPRSS2 extracellular region appeared to fold independently. The results are consistent with recently published structures of a partial TMPRSS2 extracellular fragment without the LDLR domain (60) and the full-length extracellular region of TMPRSS13 (76). N286 is located between the SRCR and the protease domains. N-glycosylation at this position seems to contribute little to the interaction with

calnexin and the folding of the neighboring modules. In supporting of this hypothesis, studies in blood coagulation factor VII also show that abolishing N-glycosylation in the protease domain, but not between an epidermal growth factor-like and the protease domains, impaired factor VII folding and secretion (77). It is noteworthy that N-glycosylation site at N250 in human TMPRSS2 is conserved in all mammals, whereas the site at N286 is conserved only in primates (Fig. S7), which probably reflects the different functional importance of these two sites observed in our study. Additional studies are required to understand the significance of N-glycosylation at N286 in primate TMPRSS2 proteins.

TMPRSS2 is believed to cleave SARS-CoV-2 S protein at the S2' site on the cell surface during viral entry, whereas cathepsins cleave the same site intracellularly after clathrin-mediated endocytosis of the viral particles (20). Considering our findings of intracellular TMPRSS2 activation and cleavage of SARS-CoV-2 S protein, it is plausible that TMPRSS2 cleaves SARS-CoV-2 S protein both extracellularly and intracellularly to promote viral entry, replication, and dissemination in host cells. Further studies will be important to verify our findings and to understand the role of TMPRSS2 at various cellular locations during SARS-CoV-2 infection.

In summary, TMPRSS2 is an epithelial TTSP critical in SARS-CoV-2 infection. In this study, we show that TMPRSS2 undergoes intracellular autoactivation and that this process is inhibited by HAI-1 and HAI-2, major inhibitors of epithelial TTSPs. N-glycosylation at an evolutionarily conserved site in the SRCR domain of TMPRSS2 is important for calnexin-assisted protein folding in the ER and subsequent intracellular trafficking, zymogen activation, and cell surface expression. Moreover, we show that TMPRSS2 cleaves SARS-CoV-2 S protein intracellularly in HEK293 cells. Our results provide new insights into the cellular mechanism in regulating TMPRSS2 biosynthesis and function. These findings may also help to elucidate the role of TMPRSS2 in major respiratory viral infection.

Experimental procedures

Plasmids

A cDNA (NM_001135099.1), encoding human TMPRSS2 (isoform 1), was amplified from Human MTC II cDNA panel (Clontech, 636743) and inserted into pcDNA 3.1/V5 plasmid (Thermo Fisher Scientific, K4800-01), as described previously (67). Site-directed mutagenesis (QuikChange Lightning, Agilent Technologies) was used to make plasmids expressing TMPRSS2 mutants N250Q, N286Q, N250Q/N286Q, R292A, and S478A. The amino acid numbering was based on the 529-amino-acid full-length TMPRSS2. All expressed TMPRSS2 proteins had a C-terminal V5 tag. The pCMV3-based plasmid, expressing the 1,287-amino-acid full-length SARS-CoV-2 S protein with a C-terminal FLAG tag, was from SinoBiological (VG40589). Plasmids expressing SARS-CoV-2 S proteins with mutated S1/S2 and S2' cleavage sites were made by site-directed mutagenesis. Plasmids expressing human corin with a C-terminal V5 tag and human HAI-1 and HAI-2 with an N-terminal FLAG tag were described previously (67,78).

Cell lines

HEK293 cells were from the American Type Culture Collection (CRL-1573, STR profiled) and grown in Dulbecco's modified Eagle's medium (DMEM) (Corning, 10-013-CVR) with 10% fetal bovine serum (FBS) (Gemini, 900-108). Human bronchial epithelial 16HBE cells (Mingzhoubio, MZ-1420, STR profiled) and human alveolar basal epithelial adenocarcinoma A549 cells (Mingzhoubio, MZ-0015, STR profiled) were grown in Minimum Essential Medium (Corning, 10-010-CV) and RPMI1640 (Corning, 10-040-CV), respectively, with 10% FBS. Cell culture was kept at 37ºC in humidified incubators with 5% CO_2.

Transfection and western blotting

HEK293, A549, and 16HBE cells in 6-well plates (Corning, 3516) were transfected with a control vector and expression plasmids using PolyJet In Vitro DNA Transfection Reagent (SignaGen Laboratories, SL100688). After 6 h, the cells were cultured in fresh medium with

10% FBS for 1-2 more days, washed with phosphate buffered saline (PBS), and lysed with 1% (v/v) Triton X-100, 50 mM Tris-HCl, pH 8.0, 150 mM NaCl, and mixed protease inhibitors (1:100, Roche Applied Science, 04693116001). Cell lysates with (reducing) or without (non-reducing) 2.5% (v/v) β-mercaptoethanol were analyzed by SDS-PAGE and western blotting with following antibodies: horseradish peroxidase (HRP)-conjugated anti-V5 (Thermo Fisher Scientific, R96125, 1:5000), HRP-conjugated anti-FLAG (Sigma, A8592, 1:10000), and anti-glyceraldehyde 3-phosphate dehydrogenase (GAPDH) (Bioworld, MB001H, 1:10000). To analyze endogenous TMPRSS2 protein in human alveolar A549 cells, an antibody against an epitope in the TMPRSS2 stem region (Abclonal, A1979, 1:500) was used in western blotting. Western blots were exposed to chemiluminescent reagents (NCM Biotech, P10050) and analyzed by an imager (Amersham Imager 600, GE Healthcare). Protein bands were quantified by densitometry.

Peptide substrate assay

A fluorogenic substate assay was used to examine TMPRSS2 catalytic activity. HEK293 cells were grown in 96-well plates and transfected with a vector (control) or plasmids expressing TMPRSS2 proteins. After 24 h at 37ºC, the cells were washed with Opti-MEM medium (Gibco, 31985050) and incubated with a fluorogenic peptide substrate (Boc-Gln-Ala-Arg-AMC, R&D Systems, ES014) (200 mM in Opti-MEM) at room temperature for 1 h. Fluorescent intensity was monitored in a plate reader (Spectra Max M5, Molecular Devices) with excitation at 380 nm and emission at 460 nm wavelengths.

Cell surface protein labeling

HEK293 cells expressing TMPRSS2 proteins in 6-well plates were washed with PBS and incubated with sulfo-NHS-biotin (0.25 mg/mL, 1 mL/well) (Thermo Fisher Scientific, 89881). After 3 min on ice, a glycine solution (100 mM, 2 mL/well) was added to stop the reaction. After 15 min, the cells were lysed. Biotin-labeled proteins were precipitated with NeutrAvidin beads (Thermo Fisher Scientific, 29201) at 4ºC. After 16 h, the beads were washed with PBS.

Proteins were eluted and analyzed by SDS-PAGE and western blotting.

Flow cytometry

HEK293 cells transfected with plasmids expressing TMPRSS2 proteins were detached from culture plates with 0.02% (w/v) EDTA and incubated with an anti-V5 antibody (Thermo Fisher Scientific, R96025, 1:500) followed with an Alexa Fluor 488-labeled secondary antibody (Invitrogen, A21202, 1: 500) or an anti-TMPRSS2 antibody (Abcam, ab280567, 1:200) followed with an Alexa Fluor 647-labeled secondary antibody (Yeasen, 33113ES60, 1:500). After washing with PBS, the cells were examined by flow cytometry (Gallios, Beckman Coulter). Pyridinium iodide (Sigma, P8080, 1:1000) was used for life cell gating. Data were analyzed with Kaluza Analysis Software (Beckman Coulter).

Immunofluorescent staining

HEK293 cells on glass coverslips were transfected with plasmids expressing TMPRSS2 proteins. After 24 h at 37ºC, the cells were fixed by 4% (v/v) paraformaldehyde (membrane non-permeable) or cold acetone (membrane permeable) at room temperature for 5 min and treated with 5% (w/v) bovine serum albumin to reduce non-specific background. Immunostaining was done using anti-V5 (Thermo Fisher Scientific, R96025, 1:500), anti-TMPRSS2 (Abcam, ab280567, 1:200), anti-KDEL (ER marker) (Abcam, ab176333, 1:500), and anti-GM130 (Golgi marker) (Abcam, ab215966, 1:1000) primary antibodies and Alexa 488 or 594-labeled secondary antibodies (Thermo Fisher Scientific, A11008 and A21203, 1:500). After washing with PBS, a solution with 4′,6-diamidino-2-phenylindole (DAPI) (Southern Biotech, 1000-20) was added to stain cell nuclei. The cells were inspected using a confocal microscope (Olympus FV3000).

Trypsin treatment of intact cells

To test if TMPRSS2 proteins were on the cell surface, HEK293 cells were transfected with plasmids expressing TMPRSS2 proteins or a control plasmid expressing corin. After 24 h at

37ºC, the cells were treated with 0.25% trypsin-EDTA (w/v) for 1 min. DMEM with 10% FBS was added to block trypsin activity. After washing with PBS, the cells were lysed. TMPRSS2 and corin proteins in cell lysates were analyzed by western blotting using an anti-V5 antibody, as described above. Similar procedures were used to examine intracellular cleavage of SARS-CoV-2 S protein by TMPRSS2.

Effects of monensin and BFA

To identify subcellular sites of TMPRSS2 activation, increasing doses of monensin (inhibitor of protein secretory pathway) and BFA (inhibitor of protein trafficking in the ER) were incubated with HEK293 cells expressing TMPRSS2. After 24 h at 37ºC, the cells were lysed and TMPRSS2 proteins in cell lysates were analyzed by SDS-PAGE and western blotting.

Glycosidase treatment

Lysates (20 µg) from A549 cells and transfected HEK293 cells expressing TMPRSS2 proteins were prepared without (non-reducing) or with (reducing) 0.5% SDS and 40 mM dithiothreitol. The samples were heated at 100ºC for 10 min. PNGase F (30 units, purified from *Flavobacterium meningosepticum*, New England Biolabs, P0704S) was added to the lysates and incubated at 37ºC for 3 h. TMPRSS2 proteins in PNGase F treated samples were analyzed by SDS-PAGE and western blotting, as described above.

Protein chase experiment

HEK293 cells in 6-well plates were transfected with plasmids expressing TMPRSS2 proteins. After 12 h at 37°C, the cells were treated with CHX (100 µg/mL) (Sigma, C7698) to stop protein synthesis. At specific time points, the cells were treated with trypsin-EDTA (0.25%) at 37°C for 1 min to remove cell surface proteins and lysed, as described above. TMPRSS2 proteins in cell lysates were examined by western blotting.

Analysis of ER chaperone interactions

To examine ER chaperone interactions, the TMPRSS2 WT and the mutants N250Q and N286Q in HEK293 cell lysates were immunoprecipitated with an anti-V5 antibody (Thermo Fisher Scientific, R96025, 1:1000) and protein A-Sepharose beads (Thermo Fisher Scientific, 101042) to pull down TMPRSS2 and associated proteins. After washing, proteins on the beads were eluted with a sample buffer containing 2.5% (v/v) β-mercaptoethanol and analyzed by SDS-PAGE and western blotting using following antibodies: anti-V5 (Thermo Fisher Scientific, R96125, 1:5000), BiP (Cell Signaling, 3177S, 1:1000), calnexin (Cell Signaling, 2679S, 1:1000), calreticulin (Cell Signaling, 12238T, 1:1000), HSP70 (Abcam, ab45133, 1:10000), and HRP-conjugated secondary antibodies (Bioworld, BS13278, 1:10000).

Inhibition of glucosidases by DNJ

HEK293 cells expressing the TMPRSS2 WT and the mutants N250Q and N286Q in six-well plates were incubated with or without DNJ (2 mM, Selleckchem, S3839), which inhibits cellular α-glucosidases I and II (57,58). After 36 h at 37 °C, the cells were washed with PBS and lysed. The lysates were used in western blotting and co-immunoprecipitation to examine TMPRSS2 activation and interactions with ER chaperones, as described above.

Cleavage of SARS-CoV-2 S protein in co-transfected cells

HEK293 cells were transfected with a vector (negative control) or plasmid expressing the full-length SARS-CoV-2 S protein alone or with the plasmid expressing TMPRSS2. After 24 h at 37ºC, the transfected cells were treated with or without trypsin, as described above, and lysed. To verify the TMPRSS2 cleavage site in the S protein, the S1/S2 and S2' site mutants were expressed in HEK293 cells without or with TMPRSS2 co-expression. The cells were lysed and S protein fragments and TMPRSS2 protein in cell lysates were analyzed by SDS-PAGE and western blotting using HRP-conjugated antibodies against FLAG and V5 tags, respectively. GAPDH on western blots were verified as a control for protein loading.

Protein 3-D structure modeling

RoseTTAFold software (https://robetta.bakerlab.org), an artificial intelligence-based deep learning program for protein structure predication (54), was used to build 3-D models to gain insights into TMPRSS2 N-glycosylation sites. The extracellular sequence of TMPRSS2 WT and mutants N250Q and N286Q (Trp143 to the C-terminus) was analyzed by RoseTTAFold. The PyMOL program (www.pymol.org) was used to generate 3-D ribbon and surface models.

Statistics

Data were analyzed with Prism 8 software (GraphPad). Normal distribution of the data was verified using Shapiro-Wilk test. If the data passed the test, comparisons among three or more groups were done using one-way ANOVA and Tukey's *post hoc* analysis. Otherwise, comparisons were done with Kruskal-Wallis test. Data are presented as mean ± SD. *P* values of < 0.05 were considered significant.

Data availability

All the data described in this study are presented in the article and accompanying supporting information.

Supporting information

This article contains supporting information.

Author contributions—Q.W. and N.D. conceptualization; Y.Z., S.S., C.D., K.H., C.Z., and M.L. methodology, investigation, and data curation; Y.Z., S.S., Q.W., and N.D. formal analysis; Y.Z., Q.W., and N.D. writing-original draft; Y.Z., S.S., C.D., K.H., C.Z., M.L., Q.W., and N.D. writing-review and editing; Q.W. and N.D. supervision and funding acquisition; All the authors read and agreed to the published version of the manuscript.

Funding and additional information—This work was supported in part by grants from the

National Natural Science Foundation of China (32171112, 81873566, and 81873840) and the Priority Academic Program Development of Jiangsu Higher Education Institutes.

Conflict of interest—The authors declare that they have no conflicts of interest with the contents of this article.

Abbreviations—The abbreviations used are: 3-D, three-dimensional; BiP, binding immunoglobulin protein; BFA, brefeldin A; CHX, cycloheximide; CoV, coronavirus; DAPI, 4′,6-diamidino-2-phenylindole; DMEM, Dulbecco's modified Eagle's medium; DNJ, 1-deoxynojirimycin; ER, endoplasmic reticulum; FBS, fetal bovine serum; GAPDH, glyceraldehyde 3-phosphate dehydrogenase; HAI, hepatocyte growth factor activator inhibitor; HAT, human airway trypsin-like protease; HEK293, human embryonic kidney 293; HRP, horseradish peroxidase; HSP, heat shock protein; IP, immunoprecipitation; LDLR, low-density lipoprotein receptor; MERS, Middle East respiratory syndrome; PBS, phosphate buffered saline; PNGase, peptide-N-glycosidase; S, spike; SARS, severe acute respiratory syndrome; SRCR, scavenger receptor cysteine-rich; TM, transmembrane; TMPRSS, transmembrane protease serine; TTSP, type II transmembrane serine protease; WB, western blotting; WT, wild type.

References

1. Paoloni-Giacobino, A., Chen, H., Peitsch, M. C., Rossier, C., and Antonarakis, S. E. (1997) Cloning of the TMPRSS2 gene, which encodes a novel serine protease with transmembrane, LDLRA, and SRCR domains and maps to 21q22.3. *Genomics* **44**, 309-320
2. Bugge, T. H., Antalis, T. M., and Wu, Q. (2009) Type II transmembrane serine proteases. *J Biol Chem* **284**, 23177-23181
3. Antalis, T. M., Bugge, T. H., and Wu, Q. (2011) Membrane-anchored serine proteases in

health and disease. *Prog Mol Biol Transl Sci* **99**, 1-50

4. Li, S., Peng, J., Wang, H., Zhang, W., Brown, J. M., Zhou, Y., and Wu, Q. (2020) Hepsin enhances liver metabolism and inhibits adipocyte browning in mice. *Proc Natl Acad Sci U S A* **117**, 12359-12367
5. Li, S., Wang, L., Sun, S., and Wu, Q. (2021) Hepsin: a multifunctional transmembrane serine protease in pathobiology. *FEBS J* **288**, 5252-5264
6. Martin, C. E., and List, K. (2019) Cell surface-anchored serine proteases in cancer progression and metastasis. *Cancer Metastasis Rev* **38**, 357-387
7. Szabo, R., and Bugge, T. H. (2020) Membrane-anchored serine proteases as regulators of epithelial function. *Biochem Soc Trans* **48**, 517-528
8. Menou, A., Duitman, J., and Crestani, B. (2018) The impaired proteases and anti-proteases balance in Idiopathic Pulmonary Fibrosis. *Matrix Biol* **68-69**, 382-403
9. Yamaoka, K., Masuda, K., Ogawa, H., Takagi, K., Umemoto, N., and Yasuoka, S. (1998) Cloning and characterization of the cDNA for human airway trypsin-like protease. *J Biol Chem* **273**, 11895-11901
10. Dong, N., Niu, Y., Chen, Y., Sun, S., and Wu, Q. (2020) Function and regulation of corin in physiology and disease. *Biochem Soc Trans* **48**, 1905-1916
11. Zhang, X., Gu, X., Zhang, Y., Dong, N., and Wu, Q. (2022) Corin: A Key Mediator in Sodium Homeostasis, Vascular Remodeling, and Heart Failure. *Biology (Basel)* **11**, 717
12. Sungnak, W., Huang, N., Bécavin, C., Berg, M., Queen, R., Litvinukova, M., Talavera-López, C., Maatz, H., Reichart, D., Sampaziotis, F., Worlock, K. B., Yoshida, M., and Barnes, J. L. (2020) SARS-CoV-2 entry factors are highly expressed in nasal epithelial cells together with innate immune genes. *Nat Med* **26**, 681-687
13. Harbig, A., Mernberger, M., Bittel, L., Pleschka, S., Schughart, K., Steinmetzer, T., Stiewe, T., Nist, A., and Böttcher-Friebertshäuser, E. (2020) Transcriptome profiling and protease inhibition experiments identify proteases that activate H3N2 influenza A and influenza B viruses in murine airways. *J Biol Chem* **295**, 11388-11407

14. Li, X., He, L., Luo, J., Zheng, Y., Zhou, Y., Li, D., Zhang, Y., Pan, Z., Li, Y., and Tao, L. (2022) Paeniclostridium sordellii hemorrhagic toxin targets TMPRSS2 to induce colonic epithelial lesions. *Nat Commun* **13**, 4331

15. Kim, T. S., Heinlein, C., Hackman, R. C., and Nelson, P. S. (2006) Phenotypic analysis of mice lacking the Tmprss2-encoded protease. *Mol Cell Biol* **26**, 965-975

16. Lucas, J. M., Heinlein, C., Kim, T., Hernandez, S. A., Malik, M. S., True, L. D., Morrissey, C., Corey, E., Montgomery, B., Mostaghel, E., Clegg, N., Coleman, I., Brown, C. M., Schneider, E. L., Craik, C., Simon, J. A., Bedalov, A., and Nelson, P. S. (2014) The androgen-regulated protease TMPRSS2 activates a proteolytic cascade involving components of the tumor microenvironment and promotes prostate cancer metastasis. *Cancer Discov* **4**, 1310-1325

17. Bose, R., Karthaus, W. R., Armenia, J., Abida, W., Iaquinta, P. J., Zhang, Z., Wongvipat, J., Wasmuth, E. V., Shah, N., Sullivan, P. S., Doran, M. G., Wang, P., Patruno, A., Zhao, Y., Zheng, D., Schultz, N., and Sawyers, C. L. (2017) ERF mutations reveal a balance of ETS factors controlling prostate oncogenesis. *Nature* **546**, 671-675

18. Tomlins, S. A., Rhodes, D. R., Perner, S., Dhanasekaran, S. M., Mehra, R., Sun, X. W., Varambally, S., Cao, X., Tchinda, J., Kuefer, R., Lee, C., Montie, J. E., Shah, R. B., Pienta, K. J., Rubin, M. A., and Chinnaiyan, A. M. (2005) Recurrent fusion of TMPRSS2 and ETS transcription factor genes in prostate cancer. *Science* **310**, 644-648

19. Li, F. (2016) Structure, Function, and Evolution of Coronavirus Spike Proteins. *Annu Rev Virol* **3**, 237-261

20. Jackson, C. B., Farzan, M., Chen, B., and Choe, H. (2022) Mechanisms of SARS-CoV-2 entry into cells. *Nat Rev Mol Cell Biol* **23**, 3-20

21. Fuentes-Prior, P. (2021) Priming of SARS-CoV-2 S protein by several membrane-bound serine proteinases could explain enhanced viral infectivity and systemic COVID-19 infection. *J Biol Chem* **296**, 100135

22. Glowacka, I., Bertram, S., Müller, M. A., Allen, P., Soilleux, E., Pfefferle, S., Steffen, I., Tsegaye, T. S., He, Y., Gnirss, K., Niemeyer, D., Schneider, H., Drosten, C., and Pöhlmann,

S. (2011) Evidence that TMPRSS2 activates the severe acute respiratory syndrome coronavirus spike protein for membrane fusion and reduces viral control by the humoral immune response. *J Virol* **85**, 4122-4134

23. Bertram, S., Glowacka, I., Müller, M. A., Lavender, H., Gnirss, K., Nehlmeier, I., Niemeyer, D., He, Y., Simmons, G., Drosten, C., Soilleux, E. J., Jahn, O., Steffen, I., and Pöhlmann, S. (2011) Cleavage and activation of the severe acute respiratory syndrome coronavirus spike protein by human airway trypsin-like protease. *J Virol* **85**, 13363-13372

24. Zang, R., Gomez Castro, M. F., McCune, B. T., Zeng, Q., Rothlauf, P. W., Sonnek, N. M., Liu, Z., Brulois, K. F., Wang, X., Greenberg, H. B., Diamond, M. S., Ciorba, M. A., Whelan, S. P. J., and Ding, S. (2020) TMPRSS2 and TMPRSS4 promote SARS-CoV-2 infection of human small intestinal enterocytes. *Sci Immunol* **5**, eabc3582

25. Zmora, P., Blazejewska, P., Moldenhauer, A. S., Welsch, K., Nehlmeier, I., Wu, Q., Schneider, H., Pöhlmann, S., and Bertram, S. (2014) DESC1 and MSPL activate influenza A viruses and emerging coronaviruses for host cell entry. *J Virol* **88**, 12087-12097

26. Zmora, P., Hoffmann, M., Kollmus, H., Moldenhauer, A. S., Danov, O., Braun, A., Winkler, M., Schughart, K., and Pöhlmann, S. (2018) TMPRSS11A activates the influenza A virus hemagglutinin and the MERS coronavirus spike protein and is insensitive against blockade by HAI-1. *J Biol Chem* **293**, 13863-13873

27. Matsuyama, S., Nagata, N., Shirato, K., Kawase, M., Takeda, M., and Taguchi, F. (2010) Efficient activation of the severe acute respiratory syndrome coronavirus spike protein by the transmembrane protease TMPRSS2. *J Virol* **84**, 12658-12664

28. Hoffmann, M., Kleine-Weber, H., Schroeder, S., Krüger, N., Herrler, T., Erichsen, S., Schiergens, T. S., Herrler, G., Wu, N. H., Nitsche, A., Müller, M. A., Drosten, C., and Pöhlmann, S. (2020) SARS-CoV-2 Cell Entry Depends on ACE2 and TMPRSS2 and Is Blocked by a Clinically Proven Protease Inhibitor. *Cell* **181**, 271-280.e278

29. Shang, J., Wan, Y., Luo, C., Ye, G., Geng, Q., Auerbach, A., and Li, F. (2020) Cell entry mechanisms of SARS-CoV-2. *Proc Natl Acad Sci U S A* **117**, 11727-11734

30. Chen, Y., Lear, T. B., Evankovich, J. W., Larsen, M. B., Lin, B., Alfaras, I., Kennerdell, J. R., Salminen, L., Camarco, D. P., Lockwood, K. C., Tuncer, F., Liu, J., Myerburg, M. M., McDyer, J. F., Liu, Y., Finkel, T., and Chen, B. B. (2021) A high-throughput screen for TMPRSS2 expression identifies FDA-approved compounds that can limit SARS-CoV-2 entry. *Nat Commun* **12**, 3907

31. Bestle, D., Heindl, M. R., Limburg, H., Van Lam van, T., Pilgram, O., Moulton, H., Stein, D. A., Hardes, K., Eickmann, M., Dolnik, O., Rohde, C., Klenk, H. D., Garten, W., Steinmetzer, T., and Böttcher-Friebertshäuser, E. (2020) TMPRSS2 and furin are both essential for proteolytic activation of SARS-CoV-2 in human airway cells. *Life Sci Alliance* **3**, e202000786

32. Li, F., Han, M., Dai, P., Xu, W., He, J., Tao, X., Wu, Y., Tong, X., Xia, X., Guo, W., Zhou, Y., Li, Y., Zhu, Y., Zhang, X., Liu, Z., Aji, R., Cai, X., Qu, D., Chen, Y., Jiang, S., Wang, Q., Ji, H., Xie, Y., Sun, Y., Lu, L., and Gao, D. (2021) Distinct mechanisms for TMPRSS2 expression explain organ-specific inhibition of SARS-CoV-2 infection by enzalutamide. *Nat Commun* **12**, 866

33. Shapira, T., Monreal, I. A., Dion, S. P., Buchholz, D. W., Imbiakha, B., Olmstead, A. D., Jager, M., Désilets, A., Gao, G., Martins, M., Vandal, T., Thompson, C. A. H., Chin, A., Rees, W. D., Steiner, T., Nabi, I. R., Marsault, E., Sahler, J., Diel, D. G., Van de Walle, G. R., August, A., Whittaker, G. R., Boudreault, P. L., Leduc, R., Aguilar, H. C., and Jean, F. (2022) A TMPRSS2 inhibitor acts as a pan-SARS-CoV-2 prophylactic and therapeutic. *Nature* **605**, 340-348

34. Bestle, D., Limburg, H., Kruhl, D., Harbig, A., Stein, D. A., Moulton, H., Matrosovich, M., Abdelwhab, E. M., Stech, J., and Böttcher-Friebertshäuser, E. (2021) Hemagglutinins of Avian Influenza Viruses Are Proteolytically Activated by TMPRSS2 in Human and Murine Airway Cells. *J Virol* **95**, e0090621

35. Hatesuer, B., Bertram, S., Mehnert, N., Bahgat, M. M., Nelson, P. S., Pöhlmann, S., and Schughart, K. (2013) Tmprss2 is essential for influenza H1N1 virus pathogenesis in mice. *PLoS Pathog* **9**, e1003774

36. Gierer, S., Bertram, S., Kaup, F., Wrensch, F., Heurich, A., Krämer-Kühl, A., Welsch, K., Winkler, M., Meyer, B., Drosten, C., Dittmer, U., von Hahn, T., Simmons, G., Hofmann, H., and Pöhlmann, S. (2013) The spike protein of the emerging betacoronavirus EMC uses a novel coronavirus receptor for entry, can be activated by TMPRSS2, and is targeted by neutralizing antibodies. *J Virol* **87**, 5502-5511

37. Zheng, X., and Sadler, J. E. (2002) Mucin-like domain of enteropeptidase directs apical targeting in Madin-Darby canine kidney cells. *J Biol Chem* **277**, 6858-6863

38. Wang, H., Zhou, T., Peng, J., Xu, P., Dong, N., Chen, S., and Wu, Q. (2015) Distinct roles of N-glycosylation at different sites of corin in cell membrane targeting and ectodomain shedding. *J Biol Chem* **290**, 1654-1663

39. Chen, S., Cao, P., Dong, N., Peng, J., Zhang, C., Wang, H., Zhou, T., Yang, J., Zhang, Y., Martelli, E. E., Naga Prasad, S. V., Miller, R. E., Malfait, A. M., Zhou, Y., and Wu, Q. (2015) PCSK6-mediated corin activation is essential for normal blood pressure. *Nat Med* **21**, 1048-1053

40. Friis, S., Uzzun Sales, K., Godiksen, S., Peters, D. E., Lin, C. Y., Vogel, L. K., and Bugge, T. H. (2013) A matriptase-prostasin reciprocal zymogen activation complex with unique features: prostasin as a non-enzymatic co-factor for matriptase activation. *J Biol Chem* **288**, 19028-19039

41. Martin, C. E., Murray, A. S., Sala-Hamrick, K. E., Mackinder, J. R., Harrison, E. C., Lundgren, J. G., Varela, F. A., and List, K. (2021) Posttranslational modifications of serine protease TMPRSS13 regulate zymogen activation, proteolytic activity, and cell surface localization. *J Biol Chem* **297**, 101227

42. Yoon, J., Cho, Y., Kim, K. Y., Yoon, M. J., Lee, H. S., Jeon, S. D., Kim, C., and Kim, M. G. (2020) A JUN N-terminal kinase inhibitor induces ectodomain shedding of the cancer-associated membrane protease Prss14/epithin via protein kinase CβII. *J Biol Chem* **295**, 7168-7177

43. Wang, L., Zhang, C., Sun, S., Chen, Y., Hu, Y., Wang, H., Liu, M., Dong, N., and Wu, Q. (2019) Autoactivation and calpain-1-mediated shedding of hepsin in human hepatoma

cells. *Biochem J* **476**, 2355-2369

44. Murray, A. S., Varela, F. A., Hyland, T. E., Schoenbeck, A. J., White, J. M., Tanabe, L. M., Todi, S. V., and List, K. (2017) Phosphorylation of the type II transmembrane serine protease, TMPRSS13, in hepatocyte growth factor activator inhibitor-1 and -2-mediated cell-surface localization. *J Biol Chem* **292**, 14867-14884

45. Martin, C. E., Murray, A. S., Mackinder, J. R., Sala-Hamrick, K. E., Flynn, M. G., Lundgren, J. G., Varela, F. A., and List, K. (2022) TMPRSS13 zymogen activation, surface localization, and shedding is regulated by proteolytic cleavage within the non-catalytic stem region. *Biol Chem* **403**, 969-982

46. Afar, D. E., Vivanco, I., Hubert, R. S., Kuo, J., Chen, E., Saffran, D. C., Raitano, A. B., and Jakobovits, A. (2001) Catalytic cleavage of the androgen-regulated TMPRSS2 protease results in its secretion by prostate and prostate cancer epithelia. *Cancer Res* **61**, 1686-1692

47. Chen, S., Wang, H., Li, H., Zhang, Y., and Wu, Q. (2018) Functional analysis of corin protein domains required for PCSK6-mediated activation. *Int J Biochem Cell Biol* **94**, 31-39

48. Dinter, A., and Berger, E. G. (1998) Golgi-disturbing agents. *Histochem Cell Biol* **109**, 571-590

49. Kataoka, H., Kawaguchi, M., Fukushima, T., and Shimomura, T. (2018) Hepatocyte growth factor activator inhibitors (HAI-1 and HAI-2): Emerging key players in epithelial integrity and cancer. *Pathol Int* **68**, 145-158

50. Ko, C. J., Hsu, T. W., Wu, S. R., Lan, S. W., Hsiao, T. F., Lin, H. Y., Lin, H. H., Tu, H. F., Lee, C. F., Huang, C. C., Chen, M. M., Hsiao, P. W., Huang, H. P., and Lee, M. S. (2020) Inhibition of TMPRSS2 by HAI-2 reduces prostate cancer cell invasion and metastasis. *Oncogene* **39**, 5950-5963

51. Tomita, Y., Matsuyama, S., Fukuhara, H., Maenaka, K., Kataoka, H., Hashiguchi, T., and Takeda, M. (2021) The Physiological TMPRSS2 Inhibitor HAI-2 Alleviates SARS-CoV-2 Infection. *J Virol*. **95**, e00434-21

52. Wang, H., Li, S., Wang, J., Chen, S., Sun, X. L., and Wu, Q. (2018) N-glycosylation in the protease domain of trypsin-like serine proteases mediates calnexin-assisted protein folding. *eLife* **7**, e35672

53. Sun, S., Wang, L., Zhang, S., Zhang, C., Chen, Y., Wu, Q., and Dong, N. (2020) N-glycan in the scavenger receptor cysteine-rich domain of hepsin promotes intracellular trafficking and cell surface expression. *Int J Biol Macromol* **161**, 818-827

54. Baek, M., DiMaio, F., Anishchenko, I., Dauparas, J., Ovchinnikov, S., Lee, G. R., Wang, J., Cong, Q., Kinch, L. N., Schaeffer, R. D., Millán, C., Park, H., Adams, C., Glassman, C. R., DeGiovanni, A., Pereira, J. H., Rodrigues, A. V., van Dijk, A. A., Ebrecht, A. C., Opperman, D. J., Sagmeister, T., Buhlheller, C., Pavkov-Keller, T., Rathinaswamy, M. K., Dalwadi, U., Yip, C. K., Burke, J. E., Garcia, K. C., Grishin, N. V., Adams, P. D., Read, R. J., and Baker, D. (2021) Accurate prediction of protein structures and interactions using a three-track neural network. *Science* **373**, 871-876

55. Helenius, A., and Aebi, M. (2001) Intracellular functions of N-linked glycans. *Science* **291**, 2364-2369

56. Ihara, Y., Cohen-Doyle, M. F., Saito, Y., and Williams, D. B. (1999) Calnexin discriminates between protein conformational states and functions as a molecular chaperone in vitro. *Mol Cell* **4**, 331-341

57. Saunier, B., Kilker, R. D., Jr., Tkacz, J. S., Quaroni, A., and Herscovics, A. (1982) Inhibition of N-linked complex oligosaccharide formation by 1-deoxynojirimycin, an inhibitor of processing glucosidases. *J Biol Chem* **257**, 14155-14161

58. Wang, H., and Wu, Q. (2019) Glucosidase Inhibition to Study Calnexin-assisted Glycoprotein Folding in Cells. *Bio Protoc* **9**, e3248

59. Essalmani, R., Jain, J., Susan-Resiga, D., Andréo, U., Evagelidis, A., Derbali, R. M., Huynh, D. N., Dallaire, F., Laporte, M., Delpal, A., Sutto-Ortiz, P., Coutard, B., Mapa, C., Wilcoxen, K., Decroly, E., Nq Pham, T., Cohen É, A., and Seidah, N. G. (2022) Distinctive Roles of Furin and TMPRSS2 in SARS-CoV-2 Infectivity. *J Virol* **96**, e0012822

60. Fraser, B. J., Beldar, S., Seitova, A., Hutchinson, A., Mannar, D., Li, Y., Kwon, D., Tan, R.,

Wilson, R. P., Leopold, K., Subramaniam, S., Halabelian, L., Arrowsmith, C. H., and Bénard, F. (2022) Structure and activity of human TMPRSS2 protease implicated in SARS-CoV-2 activation. *Nat Chem Biol* **18**, 963-971

61. Wu, C., Wu, F., Pan, J., Morser, J., and Wu, Q. (2003) Furin-mediated processing of Pro-C-type natriuretic peptide. *J Biol Chem* **278**, 25847-25852

62. Jacquinet, E., Rao, N. V., Rao, G. V., Zhengming, W., Albertine, K. H., and Hoidal, J. R. (2001) Cloning and characterization of the cDNA and gene for human epitheliasin. *Eur J Biochem* **268**, 2687-2699

63. Lu, D., Yuan, X., Zheng, X., and Sadler, J. E. (1997) Bovine proenteropeptidase is activated by trypsin, and the specificity of enteropeptidase depends on the heavy chain. *J Biol Chem* **272**, 31293-31300

64. Buzza, M. S., Martin, E. W., Driesbaugh, K. H., Désilets, A., Leduc, R., and Antalis, T. M. (2013) Prostasin is required for matriptase activation in intestinal epithelial cells to regulate closure of the paracellular pathway. *J Biol Chem* **288**, 10328-10337

65. Stirnberg, M., Maurer, E., Horstmeyer, A., Kolp, S., Frank, S., Bald, T., Arenz, K., Janzer, A., Prager, K., Wunderlich, P., Walter, J., and Gütschow, M. (2010) Proteolytic processing of the serine protease matriptase-2: identification of the cleavage sites required for its autocatalytic release from the cell surface. *Biochem J* **430**, 87-95

66. Jiang, J., Yang, J., Feng, P., Zuo, B., Dong, N., Wu, Q., and He, Y. (2014) N-glycosylation is required for matriptase-2 autoactivation and ectodomain shedding. *J Biol Chem* **289**, 19500-19507

67. Zhang, C., Zhang, Y., Zhang, S., Wang, Z., Sun, S., Liu, M., Chen, Y., Dong, N., and Wu, Q. (2020) Intracellular autoactivation of TMPRSS11A, an airway epithelial transmembrane serine protease. *J Biol Chem* **295**, 12686-12696

68. Tanaka, H., Nagaike, K., Takeda, N., Itoh, H., Kohama, K., Fukushima, T., Miyata, S., Uchiyama, S., Uchinokura, S., Shimomura, T., Miyazawa, K., Kitamura, N., Yamada, G., and Kataoka, H. (2005) Hepatocyte growth factor activator inhibitor type 1 (HAI-1) is required for branching morphogenesis in the chorioallantoic placenta. *Mol Cell Biol* **25**,

5687-5698

69. Szabo, R., Hobson, J. P., Christoph, K., Kosa, P., List, K., and Bugge, T. H. (2009) Regulation of cell surface protease matriptase by HAI2 is essential for placental development, neural tube closure and embryonic survival in mice. *Development* **136**, 2653-2663

70. Szabo, R., Uzzun Sales, K., Kosa, P., Shylo, N. A., Godiksen, S., Hansen, K. K., Friis, S., Gutkind, J. S., Vogel, L. K., Hummler, E., Camerer, E., and Bugge, T. H. (2012) Reduced prostasin (CAP1/PRSS8) activity eliminates HAI-1 and HAI-2 deficiency-associated developmental defects by preventing matriptase activation. *PLoS Genet* **8**, e1002937

71. Straus, M. R., Kinder, J. T., Segall, M., Dutch, R. E., and Whittaker, G. R. (2020) SPINT2 inhibits proteases involved in activation of both influenza viruses and metapneumoviruses. *Virology* **543**, 43-53

72. Oberst, M. D., Chen, L. Y., Kiyomiya, K., Williams, C. A., Lee, M. S., Johnson, M. D., Dickson, R. B., and Lin, C. Y. (2005) HAI-1 regulates activation and expression of matriptase, a membrane-bound serine protease. *Am J Physiol Cell Physiol* **289**, C462-470

73. Larsen, B. R., Steffensen, S. D., Nielsen, N. V., Friis, S., Godiksen, S., Bornholdt, J., Soendergaard, C., Nonboe, A. W., Andersen, M. N., Poulsen, S. S., Szabo, R., Bugge, T. H., Lin, C. Y., Skovbjerg, H., Jensen, J. K., and Vogel, L. K. (2013) Hepatocyte growth factor activator inhibitor-2 prevents shedding of matriptase. *Exp Cell Res* **319**, 918-929

74. Reily, C., Stewart, T. J., Renfrow, M. B., and Novak, J. (2019) Glycosylation in health and disease. *Nat Rev Nephrol* **15**, 346-366

75. Shakin-Eshleman, S. H., Spitalnik, S. L., and Kasturi, L. (1996) The amino acid at the X position of an Asn-X-Ser sequon is an important determinant of N-linked core-glycosylation efficiency. *J Biol Chem* **271**, 6363-6366

76. Ohno, A., Maita, N., Tabata, T., Nagano, H., Arita, K., Ariyoshi, M., Uchida, T., Nakao, R., Ulla, A., Sugiura, K., Kishimoto, K., Teshima-Kondo, S., Okumura, Y., and Nikawa, T. (2021) Crystal structure of inhibitor-bound human MSPL that can activate high pathogenic

avian influenza. *Life Sci Alliance* **4**, e202000849

77. Wang, H., Wang, L., Li, S., Dong, N., and Wu, Q. (2019) N-Glycan-calnexin interactions in human factor VII secretion and deficiency. *Int J Biochem Cell Biol* **113**, 67-74

78. Dong, N., Fang, C., Jiang, Y., Zhou, T., Liu, M., Zhou, J., Shen, J., Fukuda, K., Qin, J., and Wu, Q. (2013) Corin mutation R539C from hypertensive patients impairs zymogen activation and generates an inactive alternative ectodomain fragment. *J Biol Chem* **288**, 7867-7874

79. Gong, Y., Qin, S., Dai, L., and Tian, Z. (2021) The glycosylation in SARS-CoV-2 and its receptor ACE2. *Signal Transduct Target Ther* **6**, 396

Figure Legends

Figure 1. TMPRSS2 autoactivation in human cells. *A*, Illustration of human TMPRSS2 domains. TM, transmembrane; LDLR, low-density lipoprotein receptor; SRCR, scavenger receptor cysteine-rich. The zymogen activation site, catalytic active residues (H333, D382, and S478) in the protease domain, and a disulfide bond between the propepdie and protease domains are indicated. A V5 (*v*) tag is at the C-terminus. Predicted sizes of TMPRSS2 zymogen and the protease domain are indicated. *B*, Western blotting of TMPRSS2 in lysates from HEK293 cells transfected with a vector or a plasmid expressing TMPRSS2 WT under non-reducing (*NR*) (*left*) or reducing (*R*) (*right*) conditions. The ~65- and ~31-kDa bands are indicated by filled and open arrowheads, respectively. GAPDH was a control. *C* and *D*, Illustrations of TMPRSS2 mutants R292A (*C*) and S478A (*D*). *E*, Western blotting of the TMPRSS2 WT and the mutants R292A and S478A in lysates from transfected HEK293, 16HBE, and A549 cells under reducing conditions. *F*, Peptide substrate activities in HEK293 cells transfected with a vector or plasmids expressing the WT and the mutants R292A and S478A (n = 4). Data in *B* and *E* are representative of at least three experiments. Data in *F* are mean ± SD, analyzed by one-way ANOVA.

Figure 2. Analysis of cell surface TMPRSS2 proteins. *A* and *B*, Flow cytometric analysis of TMPRSS2 proteins on the surface of HEK293 cells transfected with a vector or plasmids expressing the TMPRSS2 WT and the mutants R292A and S478A. Percentages of TMPRSS2-positive cells are indicated (*A*). Quantitative data of FITC-positive cells (mean ± SD) from six experiments were analyzed by one-way ANOVA (*B*). *C* and *D*, Immunostaining of TMPRSS2 proteins (*green*) in HEK293 cells (*C*) and human airway 16HBE and lung A549 cells (*D*) transfected with a vector or plasmids expressing the WT and the mutants R292A and S478A. Cell nuclei were stained with DAPI (*blue*). Experiments were done under cell membrane non-permeabilized or permeabilized conditions, as indicated. Both flow cytometry and immunostaining were done using an antibody against an epitope in the TMPRSS2

exteracellular stem region. In *C* and *D*, data are representative of at least three experiments. Scale bars: 10 μm.

Figure 3. Analysis of TMPRSS2 activation cleavage in trypsin, monensin, or BFA treated HEK293 cells. *A* and *B*, Western blotting of TMPRSS2 (*A*) and corin (*B*) in lysates from transfected HEK293 without (-) or with (+) trypsin pre-treatment. The blotting was done under reducing conditions. Activation cleaved protease domain bands from TMPRSS2 (~31 kDa in *A*) and corin (~40 kDa in *B*) are indicated by open arrowheads. GAPDH was shown as a control. *C* and *D*, HEK293 cells expressing TMPRSS2 were treated with increasing doses of monensin (*C*) or BFA (*D*) at 37°C for 18 h. TMPRSS2 in cell lysates was analyzed by western blotting under reducing conditions. TMPRSS2 zymogen and cleaved protease domain bands are indicated by filled and open arrowheads, respectively. *E* and *F*, As controls, HEK293 cells expressing corin were incubated without (-) or with (+) monensin (*E*) or BFA (*F*) at 37°C for 18 h. Corin fragments in cell lysates were analyzed by western blotting under reducing conditions. Corin zymogen and cleaved protease domain bands are indicated by filled and open arrowheads, respectively. All experiments were done using an anti-C-terminal V5 tag antibody. Data are representative of at least three experiments.

Figure 4. Inhibition of TMPRSS2 activation cleavage by HAI-1 and HAI-2. HEK293 cells were transfected with a control vector or a plasmid expressing TMPRSS2 without (-) or with a plasmid expressing HAI-1 or HAI-2. TMPRSS2 fragments in cell lysates were analyzed by western blotting under reducing conditions (*R*). TMPRSS2 zymogen and protease domain bands are indicated by filled and open arrowheads, respectively (*top panel*). GAPDH (*middle panel*), HAI-1 and HAI-2 (*bottom panel*) were verified as controls by western blotting. The data are representative of three experiments.

Figure 5. Analysis of N-glycosylation in TMPRSS2. *A*, Illustration of N-glycosylation sites

in human TMPRSS2. Asn to Gln substitutions were made at 250 (*N250Q*), 286 (*N286Q*) or 250 and 286 (*N250Q/N286Q*) to abolish the N-glycosylation sites, individually or together. *B*, TMPRSS2 was expressed in HEK293 cells. Cell lysates were treated without (-) or with (+) PNGase F (*PNG F*) and analyzed by western blotting under reducing conditions. The TMPRSS2 zymogen bands at ~65 kDa (*white dot*) and ~59 kDa (*red dot*) and the protease domain band (*open arrowhead*) are indicated. Data are representative of three experiments. *C* and *D*, The TMPRSS2 WT and the mutants N250Q, N286Q, and N250Q/N286Q expressed in HEK293 cells were analyzed by western blotting under reducing conditions. The TMPRSS2 zymogen bands at ~65 kDa (*white dot*), ~62 kDa (*green dots*), and ~59 kDa (*red dot*) and the protease domain band at ~31 kDa (*open arrowhead*) are indicated. Percentages of TMPRSS2 activation cleavage, as measured by the ratios of the protease domain band *vs*. the zymogen band intensity, from six experiments were quantified. Data (mean ± SD) were analyzed by one-way ANOVA. *E* and *F*, Flow cytometric analysis of the WT and the mutants N250Q, N286Q, and N250Q/N286Q on the surface of HEK293 cells. Percentages of TMPRSS2-positive cells are shown (*E*). Quantitative data (mean ± SD) from five experiments were analyzed by one-way ANOVA (*F*).

Figure 6. Analysis of intracellular TMPRSS2 proteins in HEK293 cells. *A*, HEK293 expressing the TMPRSS2 WT and the mutants N250Q and N286Q were treated with cycloheximide (*CHX*) (100 µg/mL) at 37°C. At indicated time points, the cells were treated with trypsin to remove surface proteins. Cell lysates were prepared and analyzed by western blotting under reducing conditions. *B* and *C*, Levels of TMPRSS2 protein bands on western blots were quantified by densitometric analysis to calculate protein half-lives. Data are mean ± SD from three experiments. Statistical analysis was done by one-way ANOVA. *D*, Co-immunostaining of TMPRSS2 proteins (*green*) with the ER marker KDEL (*red*) (*left column*) or the Golgi marker GM130 (*red*) (*righ column*) in HEK293 cells transfected with a vector or plasmids expressing the TMPRSS2 WT and the mutants N250Q and N286Q. Cell nuclei were

stained with DAPI (*blue*). Data are representative of five experiments.

Figure 7. Three-dimensional (3-D) models of TMPRSS2 extracellular modules. Sequences of the extracelluar region of the TMPRSS2 WT and the mutants of N250Q and N286Q were analyzed by the deep learning RoseTTAFold program. *A*, Ribbon models of the TMPRSS2 WT and the mutants N250Q and N286Q. The LDLR (*blue*), SRCR (*yellow*), and protease (*green*) modules are displayed. *B*, Surface models of the TMPRSS2 WT and the mutants N250Q and N286Q. N250, Q250, N286, and Q286 residues are indicated.

Figure 8. Analysis of TMPRSS2 and ER chaperone interactions. *A*, Lysates were prepared from HEK293 cells expressing the TMPRSS2 WT and the mutants N250Q and N286Q. Immunoprecipitation (*IP*) was conducted using an anti-V5 tag antibody to pull down TMPRSS2 and associated proteins. Then western blotting (*WB*) was used to examine ER chaperones calnexin, BiP, calreticulin, and heat shock protein 70 (HSP70) (*rows 1-4*). TMPRSS2 proteins in the pull-down fractions (*row 5*) and in the starting cell lysates (*row 6*) and GAPDH in the starting cell lysates (*bottom row*) were verified, as controls. Data are representative of four experiments. *B*, Relative levels of calnexin, BiP, calreticulin, and HSP70 were quantified by densitometric analysis of protein bands on the western blots. Data are mean ± SD from four experiments. *P* values in calnexin, BiP, and HSP70 analysis were done by one-way ANOVA. *P* values in calreticulin analysis were done by Kruskal-Wallis test.

Figure 9. Effects of DNJ on TMPRSS2 activation and interactions with ER chaperones. *A*, HEK293 cells transfected with a vector or plasmids expressing the TMPRSS2 WT and the mutants N250Q and N286Q were treated without (-) or with (+) DNJ (2 mM), an glucosidase inhibitor. Cell lysates were prepared. TMPRSS2 fragments were analyzed by western blotting using an anti-V5 antibody under reducing conditioins. The zymogen band (*black arrowhead*) and the cleaved protease domain band (*open arrowhead*) are indicated. The data are representative of three experiments. *B*, Analysis of interactions between TMPRSS2 proteins

and ER chaperones in HEK293 cells without (-) or with (+) the DNJ treatment. Immunoprecipitation (*IP*) was done using an anti-V5 antibody to pull down TMPRSS2 and associated proteins. Western blotting (*WB*) was used to examine calnexin, BiP, and HSP70 (*rows 1-3*). TMPRSS2 proteins in the pull-down fractions (*row 4*) and in the starting cell lysates (*row 5*) and GAPDH in the starting cell lysates (*bottom row*) were verified, as controls. Data are representative of three experiments. *C*, Relative levels of calnexin, BiP, and HSP70 were quantified by densitometric analysis of protein bands on the western blots. Data are mean ± SD from three experiments. *P* values were analyzed by one-way ANOVA.

Figure 10. Intracellular cleavage of SARS-CoV-2 S protein by TMPRSS2. *A*, Illustration of SARS-CoV-2 S protein and the fragments cleaved at the S1/S2 and S2' sites. Molecular masses of the S protein fragments with a C-terminal FLAG tag (*F*) are based on amino acid sequences and predicted N-glycosylation sites. The S protein also has O-glycans (79). Actural sizes of the fragments vary depending on experimental settings. *B*, HEK293 cells were transfected with a vector or a plasmid expressing the S protein (*Spike*) without (-) or with (+) TMPRSS2 co-expression. The cells were treated without (-) or with (+) trypsin to remove surface proteins and lysed. The S protein fragments were analyzed by western blotting using an anti-FLAG antibody under reducing conditions. The S protein and the S2 and S2' fragments are indicated (*top panel*). TMPRSS2 (*middle panel*) and GAPDH (*bottom panel*) in the lysates were verified. *C*, Illustration of the S protein cleavage site mutants, in which the S1/S2 and the S2' sites were mutated, respectively. *D*, HEK293 cells transfected with a vector or plasmids expressing the S protein and the S1/S2 and S2' mutants without (-) or with (+) TMPRSS2 co-expression. The S protein fragments were analyzed by western blotting using an anti-FLAG antibody under reducing conditions (*top panel*). TMPRSS2 (*middle panel*) and GAPDH (*bottom panel*) in the lysates were verified. Data in *B* and *D* are representative of at least three experiments.

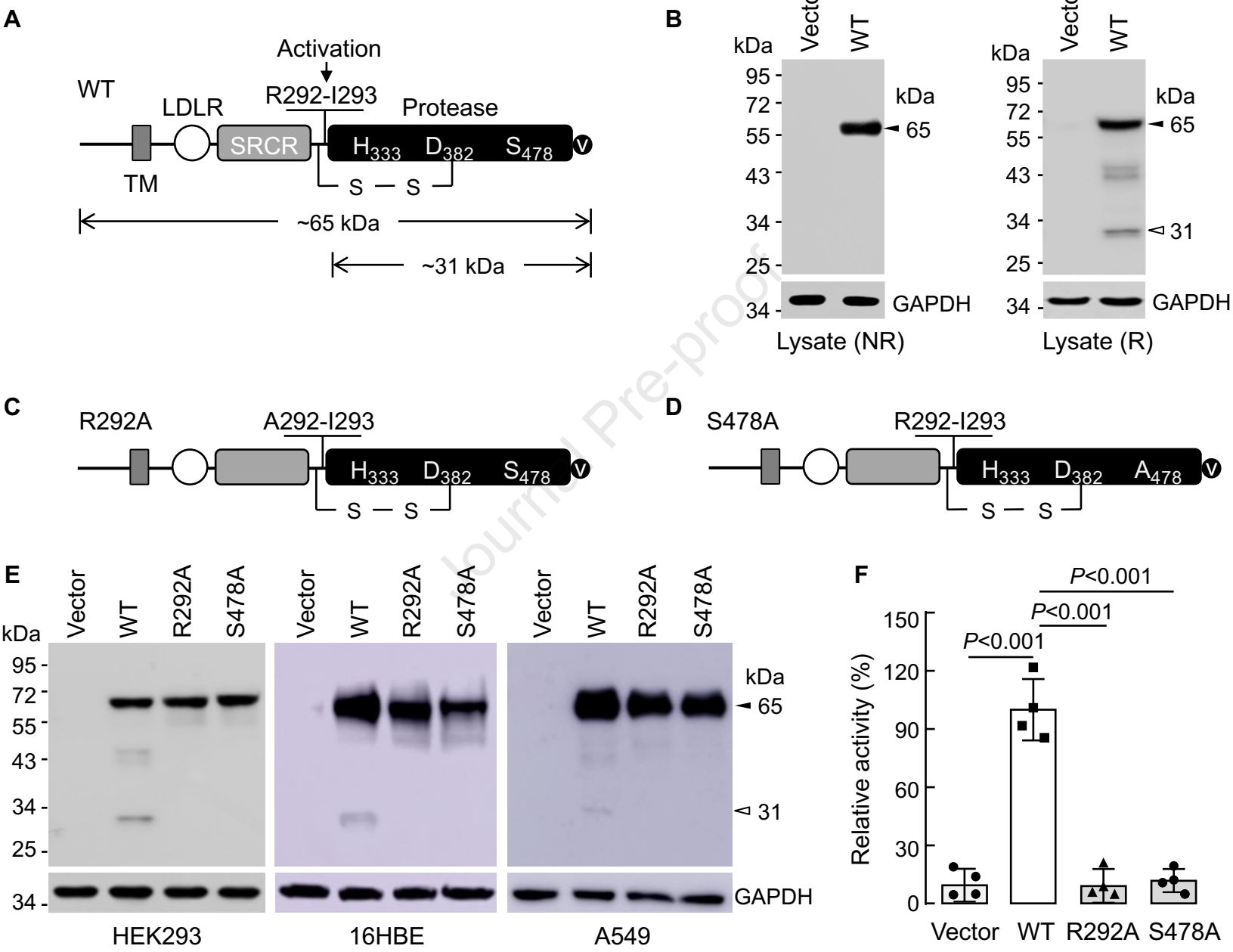

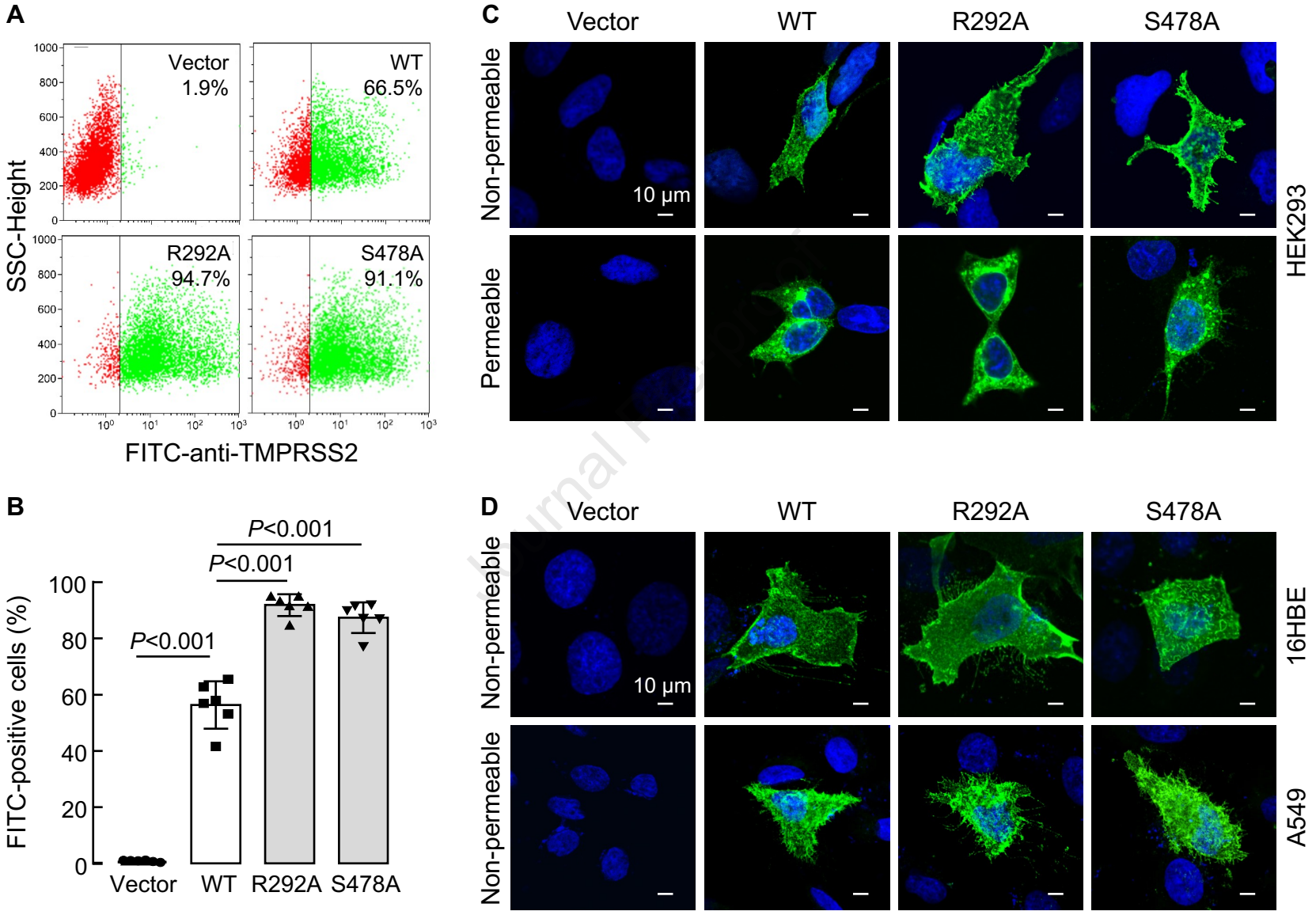
A
Vector
1.9%
WT
66.5%
R292A
94.7%
S478A
91.1%
SSC-Height
FITC-anti-TMPRSS2
B
FITC-positive cells (%)
P<0.001
P<0.001
P<0.001
Vector
WT
R292A
S478A
C
Vector
WT
R292A
S478A
Non-permeable
Permeable
10 μm
HEK293
D
Vector
WT
R292A
S478A
Non-permeable
Non-permeable
10 μm
16HBE
A549

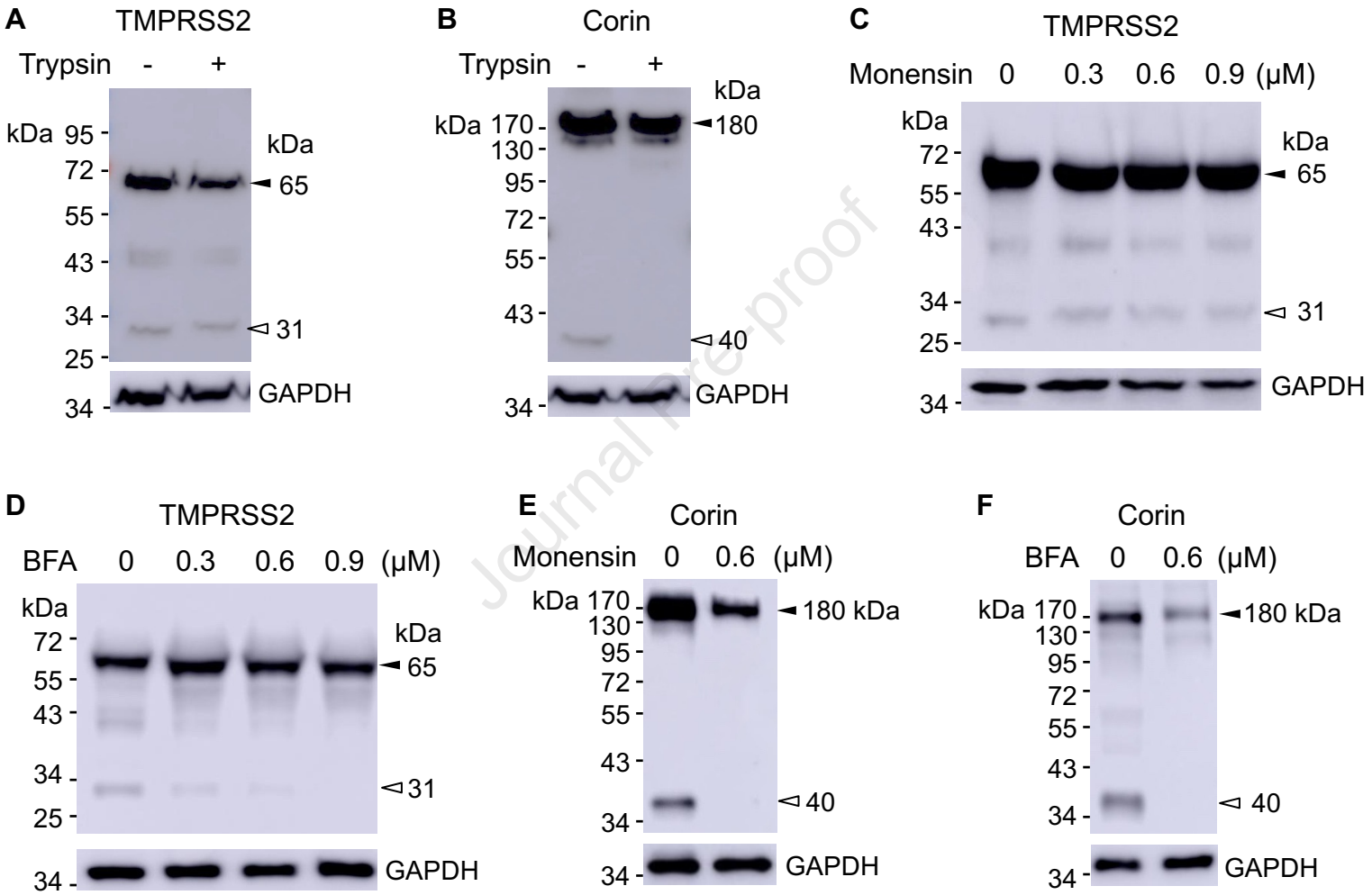

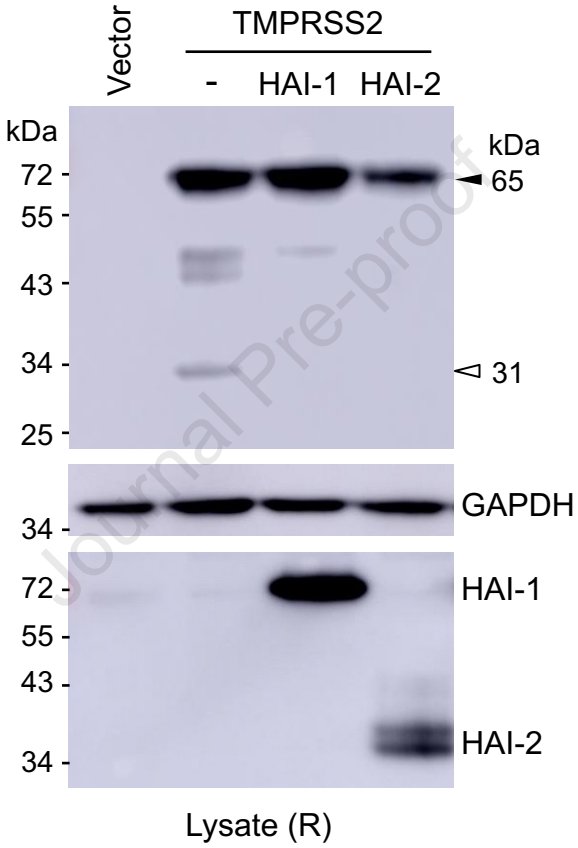

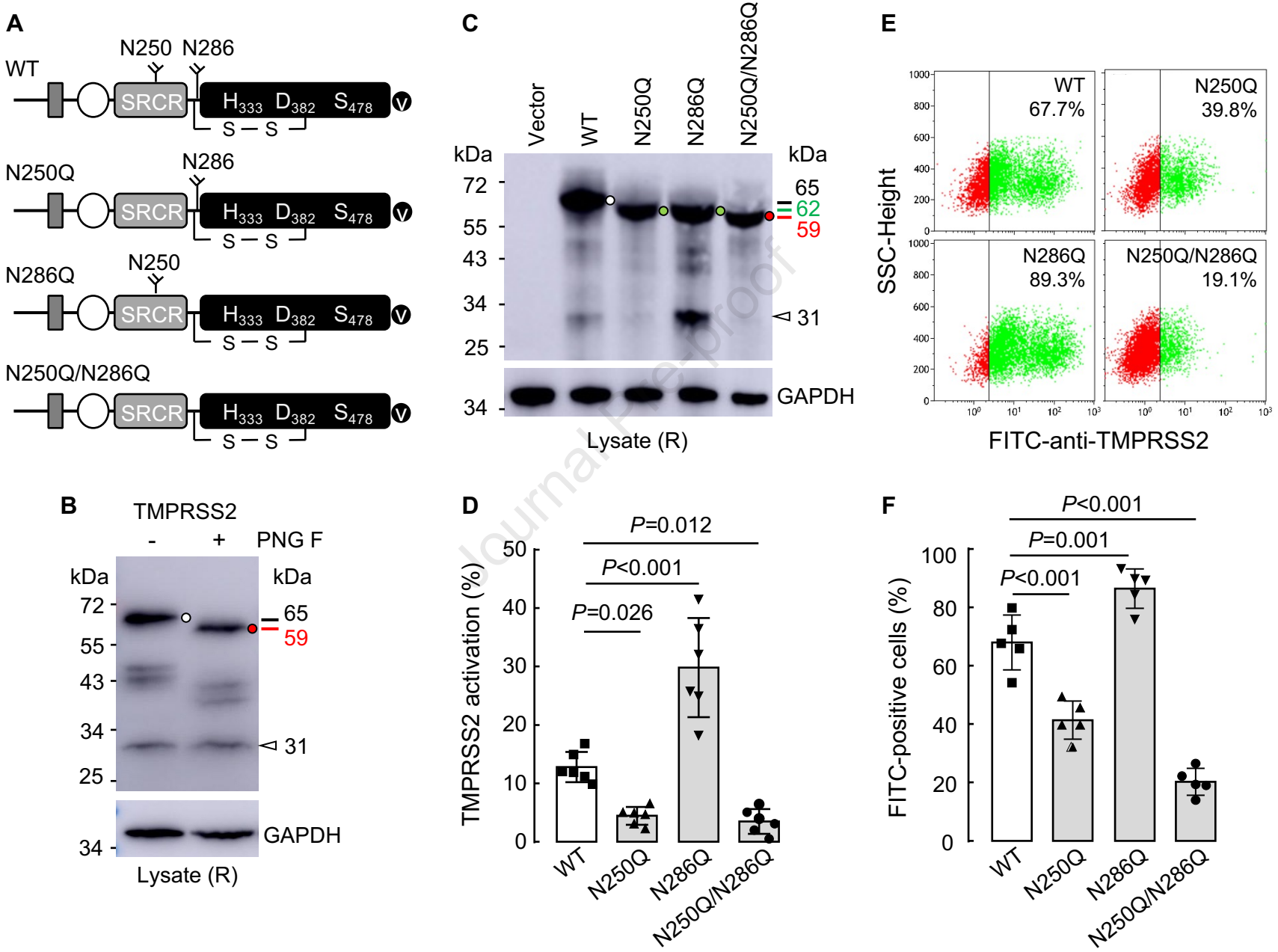
A
WT
N250
N286
SRCR
H333 D382 S478
S — S
N250Q
N286
N286Q
N250
N250Q/N286Q
B
TMPRSS2
-
+
PNG F
kDa
72
55
43
34
25
65
59
31
GAPDH
Lysate (R)
C
Vector
WT
N250Q
N286Q
N250Q/N286Q
kDa
72
55
43
34
25
65
62
59
31
34
GAPDH
Lysate (R)
D
TMPRSS2 activation (%)
P=0.012
P<0.001
P=0.026
WT
N250Q
N286Q
N250Q/N286Q
E
SSC-Height
WT
67.7%
N250Q
39.8%
N286Q
89.3%
N250Q/N286Q
19.1%
FITC-anti-TMPRSS2
F
FITC-positive cells (%)
P<0.001
P=0.001
P<0.001
WT
N250Q
N286Q
N250Q/N286Q

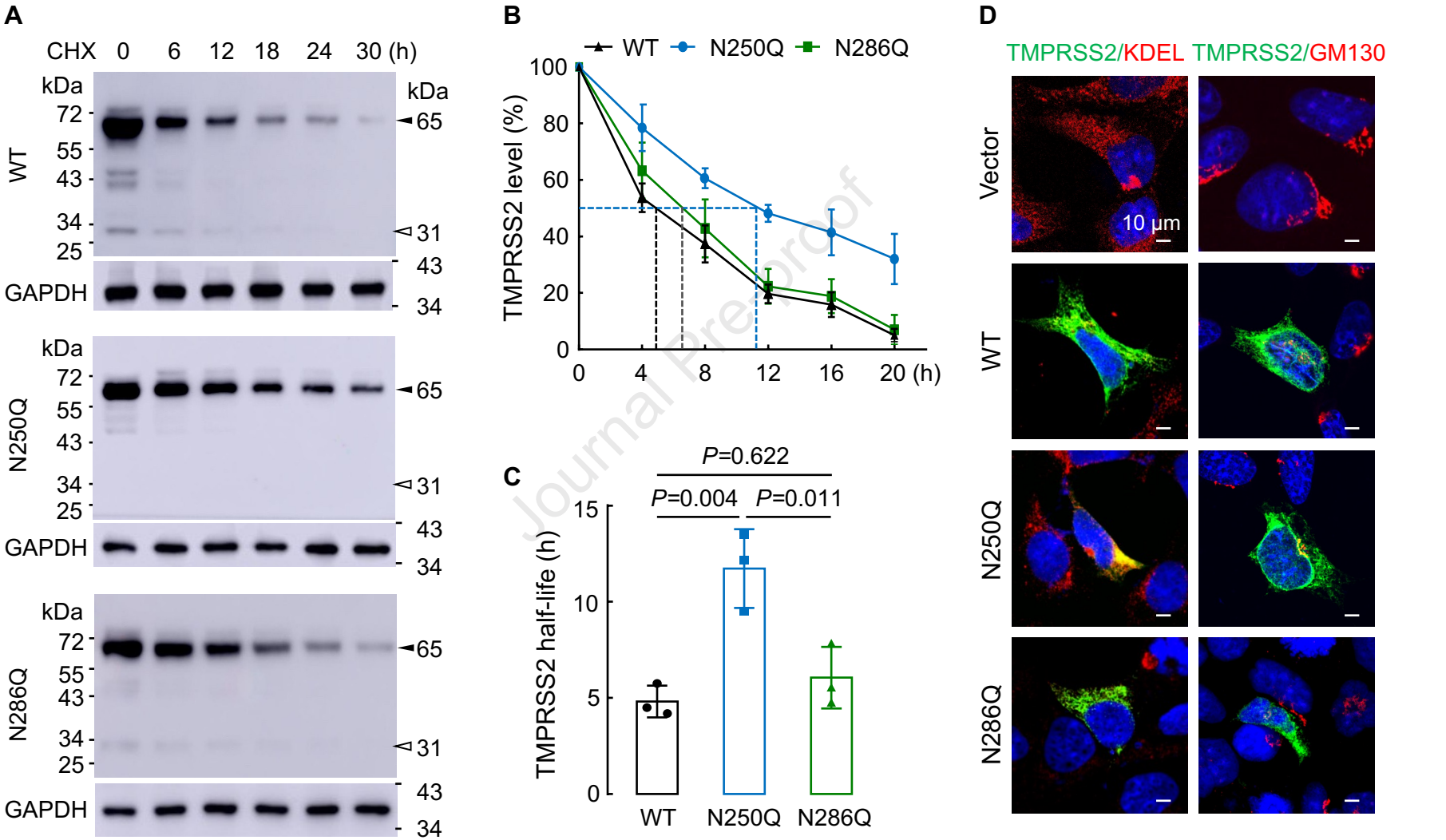

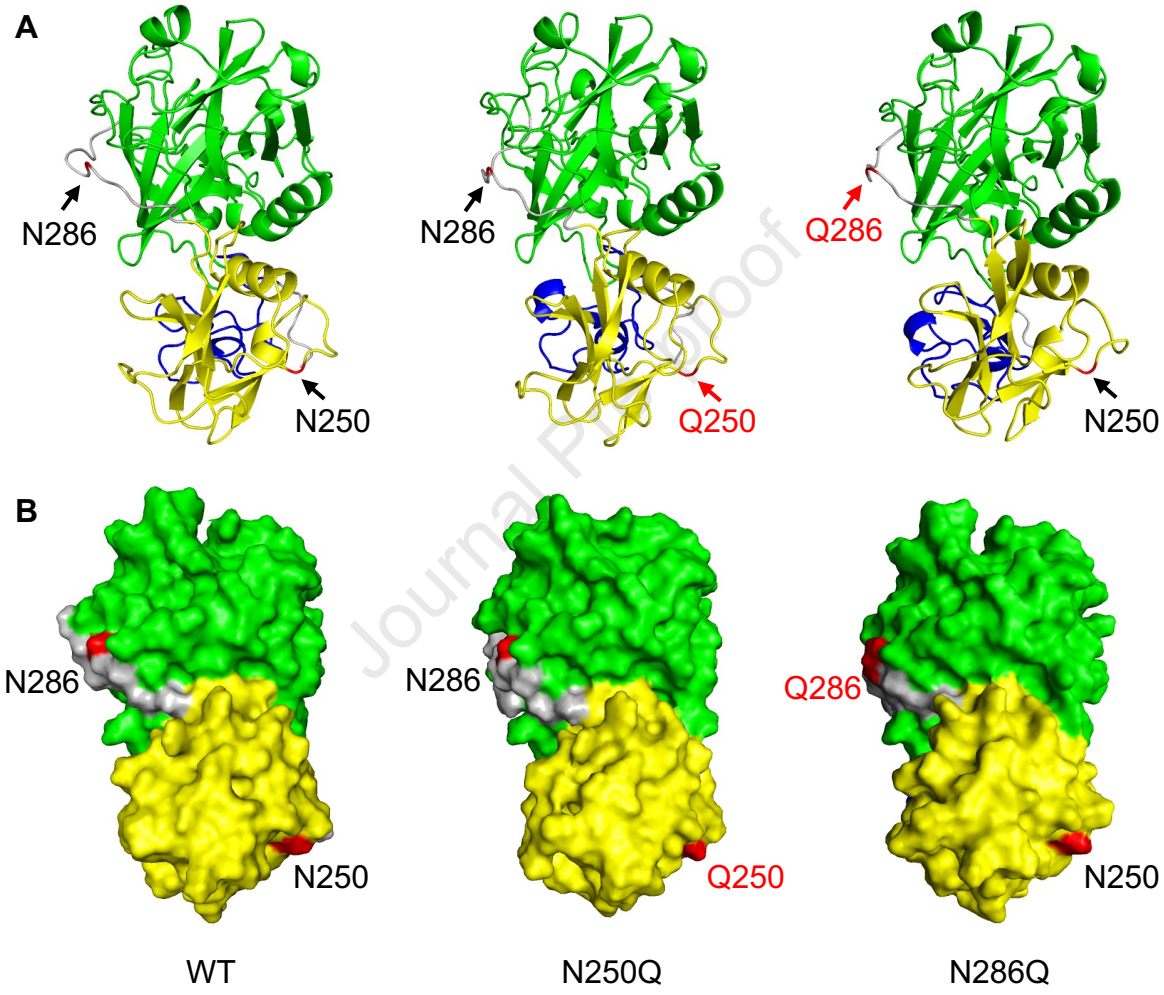

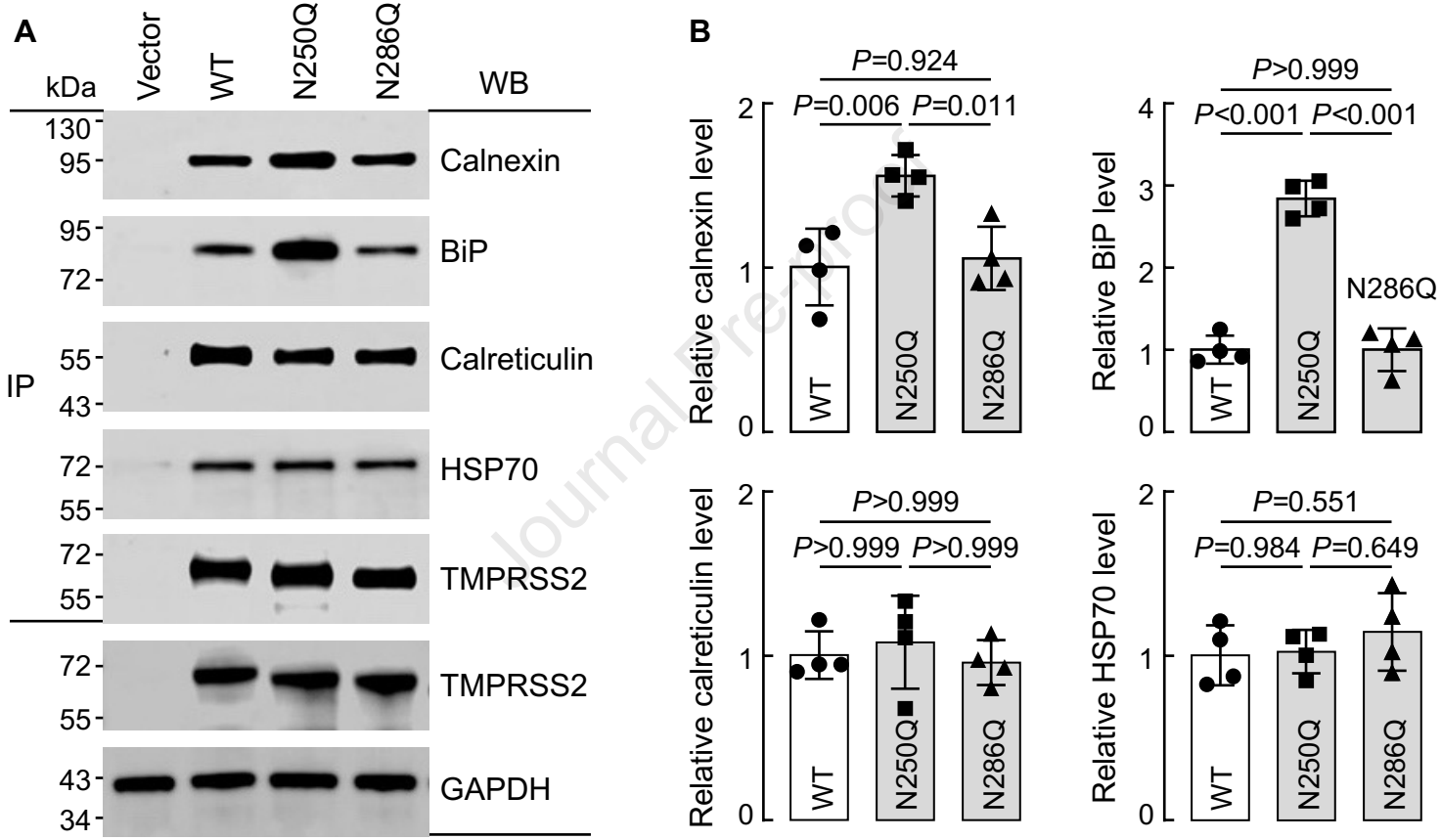

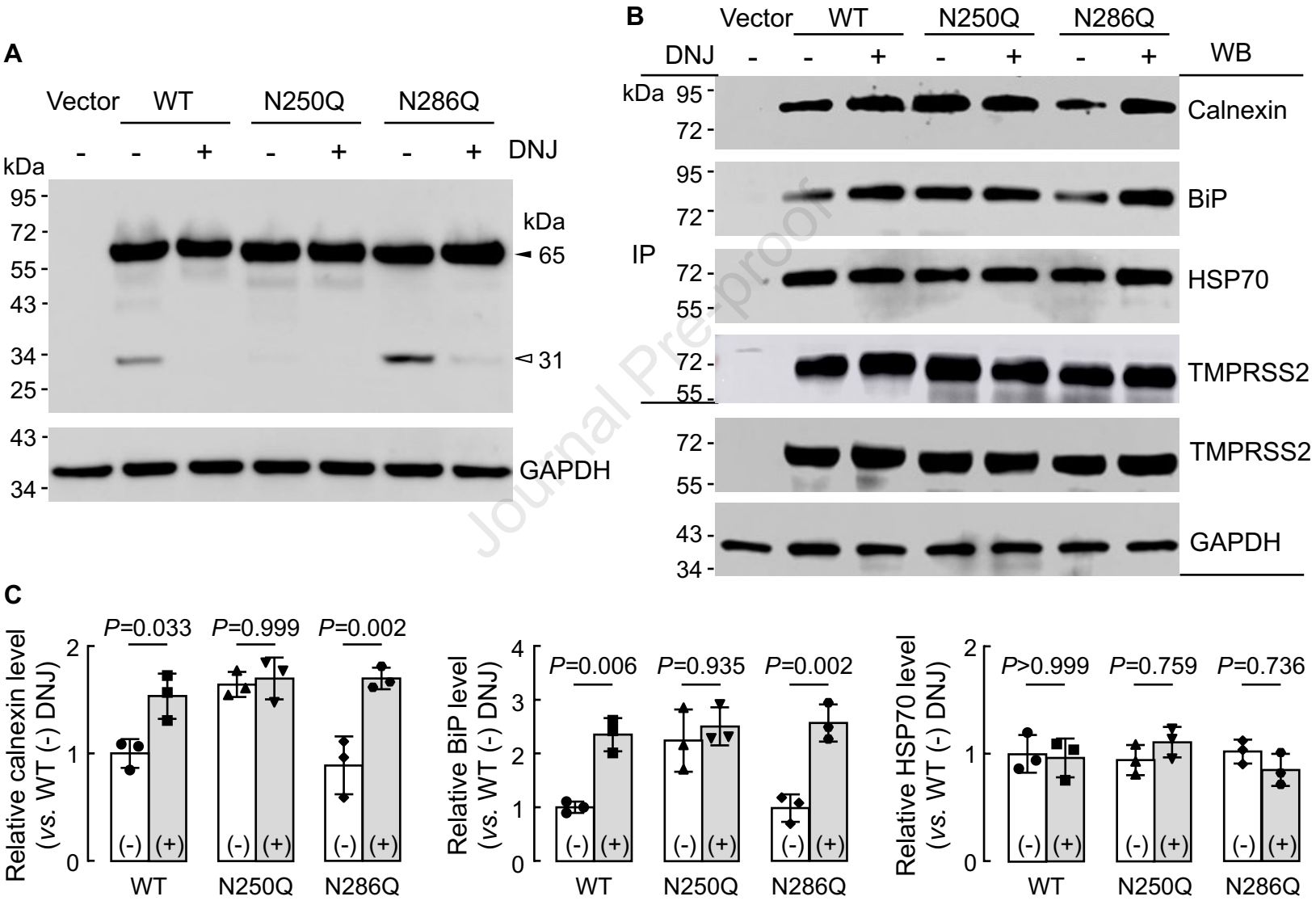

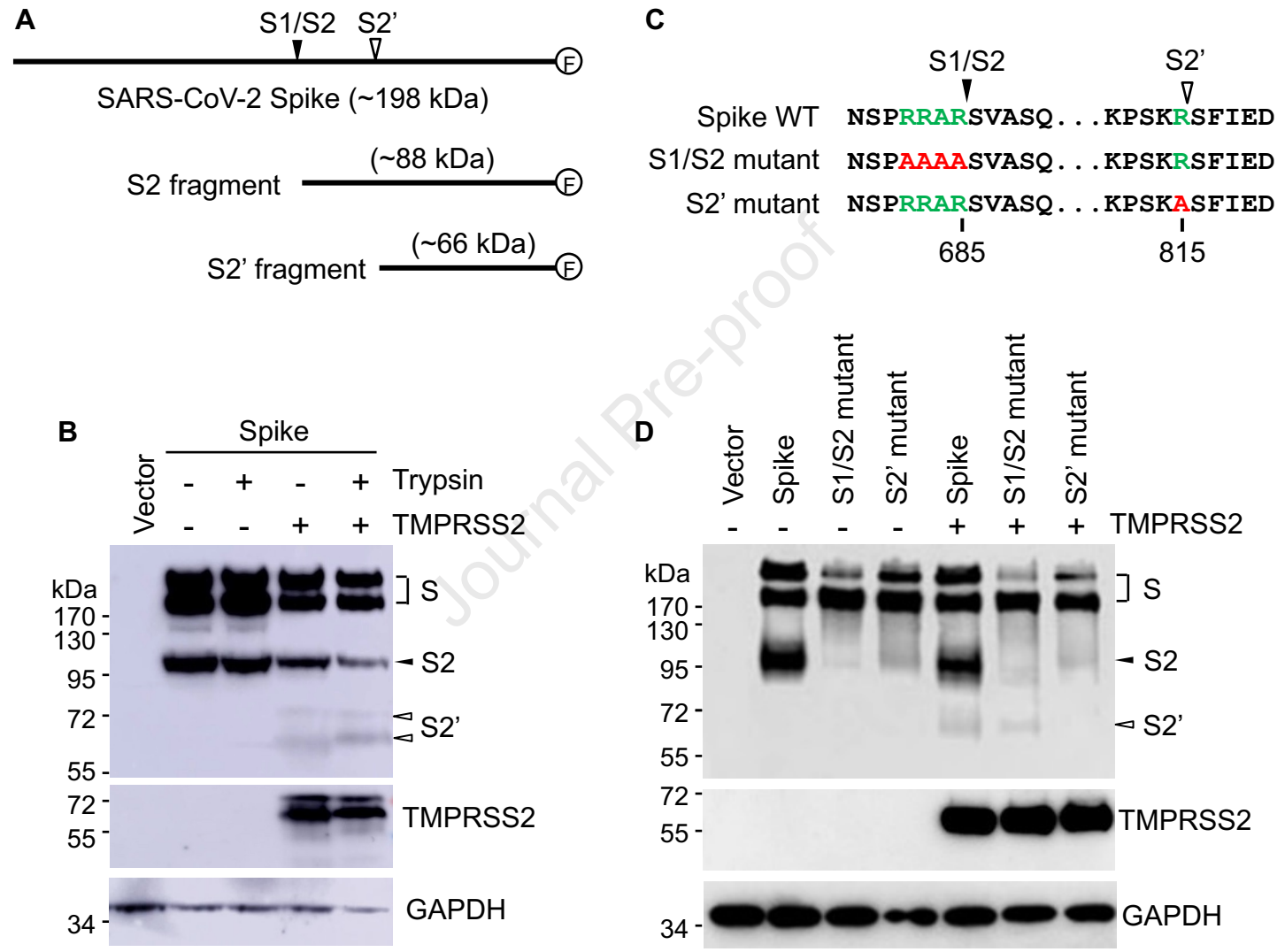

CRediT author statement

Author contributions—Q.W. and N.D. conceptualization; Y.Z., S.S., C.D., K.H., C.Z., and M.L. methodology, investigation, and data curation; Y.Z., S.S., Q.W., and N.D. formal analysis; Y.Z., Q.W., and N.D. writing-original draft; Y.Z., S.S., C.D., K.H., C.Z., M.L., Q.W., and N.D. writing-review and editing; Q.W. and N.D. supervision and funding acquisition; All the authors read and agreed to the published version of the manuscript.